Understanding how *Mycobacterium tuberculosis* Alters the T Helper Response and Identification of Novel *Staphylococcus aureus* Virulence Factors

By

Alex Henry Zilinskas

A dissertation submitted in partial satisfaction of the

requirements for the degree of

Doctor of Philosophy

in

Molecular and Cell Biology

in the

Graduate Division

of the

University of California, Berkeley

Committee in charge:
Professor Sarah A. Stanley, Chair
Professor Jeffery S. Cox
Professor Russell E. Vance
Professor Michel DuPage

Fall 2025

Abstract

Understanding how *Mycobacterium tuberculosis* Alters the T Helper Response and Identification of Novel *Staphylococcus aureus* Virulence Factors

By

Alex Henry Zilinskas

Doctor of Philosophy in Molecular and Cell Biology

University of California, Berkeley

Professor Sarah A. Stanley, Chair

Mycobacterium tuberculosis (Mtb) is an intracellular bacterial pathogen and causative agent of the disease tuberculosis. Mtb establishes infection in the lungs via inhalation of aerosol droplets containing the bacteria. Approximately a quarter of the world's population is latently infected with Mtb. Control of Mtb infection is dependent on the adaptive immune response to Mtb infection, however which cell types and immune pathways are necessary for controlling Mtb infection remains unclear. The scientific community has identified type 1 $CD4^+$ T helper cells (Th1) and their key cytokine interferon gamma (IFN-γ) as important for controlling infection, yet infected humans will eventually lose control of Mtb infection and develop active tuberculosis disease while Th1s are present in the lungs. There is growing evidence in human studies, non-human primate infection models, and murine tuberculosis vaccine models that type 17 $CD4^+$ T helper cells (Th17s) can promote control of Mtb infection, but Th17s are not always induced in Mtb infected humans and never induced in unvaccinated mice. The mechanism(s) by which Mtb-infected hosts induce Th1 and/or Th17 responses remain unclear. This highlights the necessity for understanding what are the controlling factors directing Th1 and Th17 development during Mtb infection. A more complete understanding of Th1 and Th17 development and their roles during Mtb infection will improve Mtb vaccine development which is required for eliminating the tuberculosis pandemic worldwide.

Here, we demonstrate that mice forced into a Th17 adaptive immune response are protected against Mtb infection mediated by the key cytokine produced by Th17s, IL-17a. We found that Mtb uses the type VII secretion system ESX-1 and lipid virulence factor phthiocerol dimycocerosate (PDIM) to promote infection by preventing the development of Th17s. ESX-1 and PDIM are known to be essential for the detrimental type I interferon response during Mtb infection, although the type I interferon response is not responsible

for the inhibition of Th17 development. ESX-1 and PDIM alter conventional dendritic cells in the draining mediastinal lymph node to promote expression of Th1-polarizing cytokine IL-12 and hinder expression of Th17-polarizing cytokine IL-23. These results indicate that Mtb uses the type VII secretion system ESX-1 and lipid virulence factor PDIM to force the host into a limiting but permitting Th1 adaptive immune response by preventing the development of protective Th17 cells.

Separately, *Staphylococcus aureus* (*S. aureus*) is an extracellular bacterial pathogen known to cause skin and soft tissue infections. *S. aureus* is a member of the ESKAPE pathogens known for their increasing frequency of antibiotic resistance and occurrence of infection in hospitals. The more pathogenic and antibiotic-resistant version of *S. aureus*, methicillin-resistant *S. aureus* (MRSA) causes approximately 300,000 hospitalizations and 10,000 deaths every year in the United States of America alone. MRSA contains an arsenal of virulence factors used to cause disease, however only about two-thirds of the pangenome of *S. aureus* remains consistent making virulence factor-targeted therapy difficult to design as the frequency of *S. aureus* infections being MRSA increases and the ability to use antibiotics to treat MRSA infections declines. A more comprehensive understanding of all the virulence factors used by MRSA to promote infection is required for designing novel therapeutics to treat this dangerous pathogen.

Herein, we performed a surface and secreted proteome mass spectrometry experiment and identified 21 potential hits with unknown protein function. Utilization of a genome-wide arrayed transposon library of MRSA to infect WT C57BL/6 bone marrow-derived macrophages revealed 6 out of the 21 hits with some difference in virulency compared to WT MRSA. 2 of the 6 potential virulence factors (*SAUSA300_1739* and *SAUSA300_1740*) with unknown protein functions were located next to each other in the MRSA genome. These 2 genes are located in an operon of 6 genes (*SAUSA300_1739* to *SAUSA300_1744*), which we show are transcribed together as an operon of 6 genes. Chromosomal knockouts of any of these 6 genes did not impair growth in broth, however each knockout was attenuated in a murine subcutaneous infection model. Genetic analysis of the *SAUSA300_1739* to *SAUSA300_1744* operon in several *S. aureus* strains indicate that this operon is highly conserved amongst *S. aureus* strains. And finally, we identified the protein function of SAUSA300_1739 and SAUSA300_1740 as DNases. These results reveal that MRSA uses this operon to promote infection and expands our knowledge of the arsenal of virulence factors used by MRSA.

This work is dedicated to Casey Zilinskas and Maggie Zilinskas.

Table of Contents

List of Figures

Chapter One

Chapter Two

Acknowledgements

As I approach the end of my PhD studies, I reminisce about the wonderful scientific mentors who inspired me throughout my undergraduate and graduate education. Dr. Leslie Fung provided me with the first steps into the scientific community. In Dr. Fung's lab at the University of Illinois Chicago, I learned the stringent requirements of scientific research and gained appreciation for bacterial pathogen research. Dr. Fung taught me the essentials of basic science and gave me the opportunity to explore challenging research that interested me. I hope to pay it forward as a principal investigator offering the same inspiring and devoted mentorship to enthusiastic young scientists just as Dr. Fung invested in me.

At the University of Illinois Chicago and later Tango Biosciences, Inc., Dr. Brian Kay gave me the opportunity to progress my scientific education forward. Dr. Kay provided me with insight into the public academic and private biotechnology worlds. In Dr. Kay's lab and business, I learned several lab techniques and gained appreciation for converting basic science into potential therapeutics to treat diseases ranging from autoimmune diseases, neurological diseases, and cancer. I would like to give special thanks to Dr. Jennifer McGinnis and Christina Miller for their mentorship and cheerful discussion. Dr. Fung and Dr. Kay were the mentors who fostered my eagerness to learn new fields of science, strength to accomplish difficult and exhausting scientific experiments, and desire to design novel therapeutics to treat human diseases.

At the University of California, Berkeley, I joined Dr. Sarah Stanley's lab to work on my thesis during the COVID-19 pandemic. Graduate school during the pandemic was a challenge, however I greatly appreciate Sarah's mentorship and willingness to allow me to explore scientific questions with a large degree of independence. Sarah, I am extremely grateful for the opportunities and mentorship you have provided me with during my graduate studies. I cherish the helpful and lively discussions with previous lab members Dr. Doug Fox, Dr. Erik Van Dis, Xammy Nguyenla, Dr. Robyn Jung, Dr. Marietta Ravesloot-Chavez, Sagar Rawal, Helia Samani, Dr. Daniel Fines, Dr. Ronald Rodriguez, Noah Baker, Dr. Ira Jain, and Dr. Sam Berry. I want to give a special thanks to Dr. Doug Fox. Doug, your guidance and help through the hardships of graduate school have been unbelievably helpful to me. As well, I also appreciate the current lab members of the Stanley lab: Andrea Anaya-Sanchez, Scott Espich, Nick Campbell-Kruger, Dr. Rishika Baral, Lillian Shallow, Amir Balakhmet, Isabel Lamb-Echegaray, Sydnee Gould, Carolina Agudelo, Samantha Liu, and Dr. Kayla Dinshaw.

Next, I would also like to thank several faculty at UC Berkeley: Dr. Jeff Cox, Dr. Russell Vance, Dr. Michel DuPage, and Dr. Dan Portnoy. You have all given me valuable insight into scientific experimental design and offered words of encouragement over the course of my PhD. I would like to thank several fellow graduate students and post-doctoral fellows. Dr. Nick Garelis, Dr. Allison Roberts, and Dr. Zoe Netter in the Cox lab have graciously offered their thoughts, protocols, and help to me throughout my graduate

studies. Stephanie Silveria, Tim Campbell, Dr. Sebastian Fernandez, and Dr. Jessie Garcia-Castillo from or currently in the DuPage lab have assisted me with flow cytometry protocols and troubleshooting, along with positive discussions throughout graduate school.

Lastly, I want to give special thanks to Dr. Sebastian Fernandez and Dr. Jesse Garcia-Castillo for all the times we socialized outside of work. You both gave me helpful advice about the ins-and-outs of graduate school. Jesse, you have always been a thoughtful and selfless mentor who gave me so much mentorship even though you had no obligations to help me. I hope to continue our friendship after grad school. I would like to give a last thanks to Christina Miller. Christina, we've been though a lot of hardships together. You have always been an ear to speak to, and I greatly appreciate your friendship through good and hard times. I can't wait to turn this thesis in, graduate, and go on that Taiwan trip I promised you! Filled with anxiety and excitement, I can't wait for what comes next in my life. I appreciate all the help everyone I met in my undergraduate studies, graduate education, and personal life gave me to become the scientist I am today.

Chapter One: *Mycobacterium tuberculosis* (Mtb) uses the type VII secretion system ESX-1 and lipid PDIM to suppress the development of a protective Th17 response

This work is currently in review in eLife and has been submitted on BioRxiv:
Zilinskas A, Balakhmet A, Fox D, Ni HM, Agudelo C, Samani H, Stanley SA. Mycobacterium tuberculosis suppresses protective Th17 responses during infection. doi: https://doi.org/10.1101/2025.05.08.652811

Abstract

Mycobacterium tuberculosis (Mtb) causes more deaths annually than any other single pathogen, yet an effective vaccine remains elusive. IFN-γ-producing CD4+ T cells are necessary but insufficient for protection against infection. In humans, the development of IL-17A producing Th17 T cells correlates with protection, however not all individuals develop a Th17 response. In mice, experimental vaccines can elicit protective Th17 cells, yet Th17s are rare in primary infection. Why Mtb fails to consistently elicit Th17s is unknown. Here, we identify factors suppressing Th17 responses during primary infection. We demonstrate that the lack of Th17 induction is independent of route and duration. Next, using Tbet deficient mice, we show that Mtb drives a Th1 response that is only partially protective and limits Th17 cell production in an IFN-γ independent manner. We further reveal that the ESX-1 type VII alternative secretion system and lipid PDIM suppresses Th17 responses. Infection with ESX-1 or PDIM mutants results in significantly increased Th17 T cells and IL-17A cytokine in the lungs, and infection of IL-17A deficient animals partially restores virulence of ESX-1 and PDIM mutants. Although the ESX-1 secretion system and lipid PDIM elicits type I IFN, which can suppress Th17 differentiation, we find that suppression of Th17 is independent of type I IFN. Instead, ESX-1 and PDIM suppresses production of IL-23, a cytokine that promotes Th17 differentiation, in dendritic cells found in mediastinal lymph nodes during Mtb infection. These findings define a new function of the ESX-1 secretion system and PDIM in Mtb virulence, a long-standing question in tuberculosis research.

Introduction

Mycobacterium tuberculosis (Mtb), the causative agent of tuberculosis (TB), remains one of the leading infectious disease killers worldwide, with 10.8 million new cases and 1.25 million deaths reported in 2021 (1). The current vaccine, *Mycobacterium bovis bacillus Calmette-Guérin* (BCG), protects against childhood TB, but has highly variable efficacy, wanes over time, and provides minimal protection against adult pulmonary TB (1–3). Although there are 17 vaccine candidates currently in clinical trials, achieving robust vaccine elicited immunity remains a major challenge (4).

Interferon-γ (IFN-γ) produced by type 1 T helper (Th1) cells is essential for control of Mtb infection both in animal models and in humans (5, 6). However, the MVA85A vaccine, despite inducing robust Th1 responses as intended, failed to provide protection against Mtb infection (7). Patients with active TB can have high levels of IFN-γ in the lungs despite being unable to control infection (8). Thus, Th1 cells are necessary but not sufficient for controlling Mtb infection suggesting that other factors are important for effective immunity. Without a comprehensive understanding of which types and specific subsets of T helper cells are essential to limit Mtb infection, developing an effective Mtb vaccine with consistent high efficacy will remain elusive.

Type 17 T helper (Th17) cells are known for their association with mucosal sites, including the lungs, where they have been shown to provide protection against several bacterial and fungal respiratory pathogens (9). This protection relies on IL-17A production by Th17 cells (10). Many factors determine whether Th17 cells are elicited by infection. Antigen-presenting cells (APCs) drive the polarization of naïve T cells into Th17 cells by producing cytokines including IL-1β, IL-6, TGF-β, and IL-23. Activation of the RORγT transcription factor is essential for Th17 polarization (11). There is also evidence that the route of infection influences whether a Th17 response is elicited as infection with *Listeria monocytogenes* via the intranasal, but not intravenous route is required to observe a Th17 response to infection (12).

Th17 differentiation is opposed by Th1 differentiation via multiple mechanisms. Tbet, the transcription factor essential for commitment to the Th1 lineage, has been shown to prevent Runx1 activation, thereby preventing Runx1-mediated transactivation of RORγT and Th17 differentiation (11). Additionally, IFN-γ, the signature cytokine of Th1s, inhibits Th17 differentiation and function via activation of STAT1, independent of Tbet (13). Finally, production of type I IFN also can suppress Th17 differentiation (14). Thus, several hallmarks of Mtb infection, namely strong Th1 responses, IFN-γ production, and type I interferon production could limit differentiation of Th17s.

Increasing evidence that Th17 cells correlate with protection against Mtb infection both in the non-human primate model (15) and in humans (16–18) suggest that Th17 cells are an important component of protective immunity to Mtb. In mice, Th17 cells are rarely observed during primary Mtb infection, and the conditions under which Th17 cells are induced during infection remain unclear (19). However, experimental TB vaccines,

particularly when administered via a mucosal route, elicit Th17 cells that can confer protection against subsequent challenge in mice (20–22), demonstrating that Th17 cells can be protective against Mtb infection. Why Mtb infection does not robustly elicit Th17 cells during primary infection, despite causing infection at mucosal surfaces via airway infection, is unclear.

The ESX-1 type VII alternative secretion system is a fundamental determinant of Mtb virulence (23). The ESX-1 secretion system has been demonstrated to subvert and/or manipulate immune responses, including by perforating phagosomal membranes, inducing detrimental host type I interferon, and inducing autophagy (24–26). As much of the work examining ESX-1 function has been conducted in vitro, we lack a clear understanding of all the factors that attenuate ESX-1 mutants during in vivo infection. Interestingly, the Mtb lipid phthiocerol dimycocerosate (PDIM) is also required for virulence and has been linked to ESX-1 function through induction of type I IFN, which can suppress Th17 responses (27, 28). Furthermore, the ESX-1 secretion system was shown to suppress production of IL-12 p40 (23), a subunit shared with IL-23, which promotes Th17 differentiation. These data suggest that Mtb virulence factors, including ESX-1 and PDIM, may suppress the emergence of a protective Th17 response during Mtb infection.

Here we show that the induction of Th17 cells during Mtb infection is suppressed by multiple mechanisms. First, we show that the absence of a Th17 response during primary infection is not dependent on duration or route of infection. Instead, we show that mice lacking Tbet (*Tbx21*$^{-/-}$) produce Th17 cells after Mtb infection, and that these cells provide IL-17A-dependent protection against early Mtb infection. This suppression of Th17 production by Th1 cells is independent of IFN-γ. Furthermore, we observe a strong Th17 response during infection with ΔESX-1 or PDIM-lacking Mtb in naïve mice, suggesting that these virulence factors function to suppress Th17 differentiation. Surprisingly, the ability of ESX-1/PDIM to suppress Th17 differentiation is not related to their enhanced induction of type I IFN. Instead, we show that during infection with ΔESX-1 or PDIM-lacking Mtb strains type 2 conventional dendritic cells (CD11b^{+} DCs, cDC2s), which are known to support Th17 differentiation, produce higher levels of IL-23 secretion in draining lymph nodes of Mtb infected mice (29). These results demonstrate that Mtb utilizes the ESX-1 secretion system and PDIM to bias host T helper response towards Th1s and away from Th17s.

Materials and Methods

Ethics statement

All procedures involved with the use of mice were approved by the University of California, Berkeley's Institutional Animal Care and Use Committee (protocol 2015-09-7979). All protocols conform to federal regulations, the National Research Council Guide for the Care and Use of Laboratory Animals, and the Public Health Service Policy on Humane Care and Use of Laboratory Animals.

Bacterial Culture

Mycobacterium tuberculosis strain Erdman was grown in Middlebrook 7H9 liquid medium supplemented with 10% oleic acid, albumin, dextrose, and catalase (OADC) (BD 212351), 0.4% glycerol, and 0.05% Tween 80 or on solid 7H10 agar plates supplemented with 10% OADC and 0.4% glycerol. Frozen stocks of *M. tuberculosis* were made from a single culture and used for all experiments.

Mice

C57BL/6J (no. 000664), *Ifng*$^{-/-}$ (B6.129S7-*Ifng*^{tm1Ts}/J, no. 002287), *Tbet*$^{-/-}$ (*Tbx21*$^{-/-}$, B6.129S6-*Tbx21*^{tm1Glm}/J, no. 004648), and *Il17a*$^{icre/icre}$ (*Il17a*$^{-/-}$, B6.129(SJL)-*Il17a*$^{tm1.1(icre)Stck}$/J, no. 035717) mice were obtained from The Jackson Laboratory and bred in-house. *Ifnar1*$^{-/-}$, *Sp140*$^{-/-}$, and *Sp140*$^{-/-}$*Ifnar1*$^{-/-}$ mice were obtained from the Vance laboratory (UC Berkeley) and bred in-house. Mice were age matched for all experiments.

Aerosol challenge experiments with *M. tuberculosis*

Mice between the ages of 8 and 12 weeks old were infected via the aerosol route with *M. tuberculosis* strain Erdman using a nebulizer and full-body inhalation exposure system (Glas-Col, Terre Haute, IN). A total of 9 mL of diluted aerosol stock in MilliQ water was loaded into the nebulizer to deliver 30-100 bacteria per mouse as measured by whole lung CFU 1 day post-infection.

Intranasal challenge experiments with *M. tuberculosis*

Mice between the age of 8 to 12 weeks old were infected with 40 uL of *M. tuberculosis* strain Erdman diluted in PBS administration for mice to inhale 30-100 bacteria per mouse as measured by whole lung CFU 1 day post-infection.

Flow Cytometry

Whole lungs were homogenized using GentleMACS C tubes (Miltenyi Biotec 130-093-237) in complete RPMI-1640 media supplemented with 10% FBS, 1 mM sodium pyruvate (Sigma Aldrich S8636), 0.01 mM HEPES, 1% Glutamax (Thermo Scientific 35050061),

1% non-essential amino acids (Gibco 11140-050), and 55 µM 2-mercaptoethanol (Gibco 21985-023) containing Liberase TM (Sigma Aldrich 05401119001) and DNase I (Sigma Aldrich 11284932001). Cells were strained through 70 micron strainer (Corning 352350). Cells were treated with protein transport inhibitor cocktail mix (Invitrogen 00-4980-03) and stimulated with vehicle control, Mtb Ag85b peptide pool (Peptides&elephants LB02088), Mtb esat6 peptide pool (Peptides&elephants LB02113), or PMA and ionomycin (Invitrogen 00-4970-93) for 5 hours at 37 ^{o}C, 5% CO_2. Cells were stained with live/dead stain (ThermoFisher L23101), Fc block (Biolegend 101320), and surface stained with antibodies for CD3, Ly6G, CD4 (BD 740268, 551460, and 569182 respectively), MHC-II, pan-γδTCR, and CD8a (Biolegend 107605, 118124, and 100714 respectively) in Brilliant stain buffer (BD 566349). Cells were fixed and permeabilized with Foxp3 staining kit (Invitrogen 00-5523-00) before intracellular staining for RORγT, Foxp3 (BD 564723 and 562996 respectively), Tbet, IFN-γ, and IL-17A (Biolegend 644817, 505814, and 506903 respectively). Data was collected using a BD Symphony A3 flow cytometer (BD) and analyzed using FlowJo Software (BD).

Mediastinal lymph nodes were homogenized using complete RPMI-1640 containing Liberase TM (Sigma Aldrich 05401119001) and DNase I (Sigma Aldrich 11284932001) with sterile plunger of 3 mL syringe to pass dissociated tissue through 100 micron cell strainer (Corning 352360). Cells were stained with live/dead stain (ThermoFisher L34966), Fc block (Biolegend 101320) and surface stained with antibodies for XCR1, CD11b, CD11c, Ly6G, MHC-II, CD3, CD19 (Biolegend 148220, 101261, 117318, 127627, 107606, 100233, and 115545 respectively) and Ly6C and CD64 (BD 755198 and 569507 respectively) in Brillant stain buffer (BD 566349). Cells were fixed and permeabilized with Foxp3 staining kit (Invitrogen 00-5523-00) before intracellular staining for IL-12 p35 (Invitrogen MA5-23559) and IL-23 p19 (BD 565317). Data were collected using a BD Symphony A3 flow cytometer (BD) and analyzed using FlowJo Software (BD).

For Legendplex, whole lungs were homogenized using 70 micron cell strainer (Corning 352350) and plunger of 3 mL syringe into complete RPMI. Single cell suspensions were pelleted at 1200 rpm for 5 minutes at 4 ^{o}C. Supernatants were collected for LEGENDplex with pre-made mouse inflammation panel (13-plex) (Biolegend 740446). Prior to final wash and running on flow cytometer, beads were fixed with 4% PFA and plate transferred to BSL1. Data was collected using a BD Symphony A3 flow cytometer (BD) and analyzed using LEGENDplex Data Analysis Software Suite (Biolegend).

Lung homogenate protein concentration measurements

Whole lungs were homogenized in complete RPMI-1640 media supplemented with 10% FBS, 1 mM sodium pyruvate (Sigma Aldrich S8636), 0.01 mM HEPES, 1% Glutamax (Thermo Scientific 35050061), 1% non-essential amino acids (Gibco 11140-050), and 55 µM 2-mercaptoethanol (Gibco 21985-023) and meshed through 70 micron cell strainer (Corning 352350) with plunger of 5 mL syringe. Cells were pelleted at 1,500 rcf for 5

minutes and supernatants were collected for measuring protein concentrations with BioLegend LEGENDplex mouse inflammation panel (13-plex) (Biolegend 740446).

Exogeneous IL-17A administration

Mice were intranasally administered 1 µg endotoxin-free recombinant murine IL-17A (R&D systems, 7956-ML-100/CF) in 40 µL sterile PBS daily or 40 µL of vehicle control daily, or intraperitoneally administered 2 µg endotoxin-free recombinant murine IL-17A in 100 µL sterile PBS daily or 100 uL of vehicle control dailiy from days 11 to 20 post aerosol *M. tuberculosis* challenge.

MSA-IL-17A was generated by fusing a (GGGGS)3 linker between the C-terminus of mature murine serum albumin and N-terminus of mature murine IL-17A. MSA-IL-17A was purchased from Genscript USA, Inc. in endotoxin-free pH 7.2 PBS. Mice were intranasally administered 5.54 µg MSA-IL-17A (equimolar to 1 µg recombinant murine IL-17A) in 40 µL sterile PBS daily or 40 µL vehicle control, or intraperitoneally administered 11.09 µg MSA-IL-17A (equimolar to 2 µg recombinant murine IL-17A) in 100 µL PBS or 100 µL vehicle control daily between days 11 to 20 post aerosol *M. tuberculosis* challenge.

Bone-marrow-derived macrophage infection

WT C57BL/6J bone-marrow-derived macrophages (BMDMs) were incubated on tissue-culture plates for 48 hours prior to infection at 37 ^{o}C, 5% CO_2. BMDMs were spin-fected at 1200 rpm for 10 minutes at room temperature for an MOI of 10. BMDMs were washed with 1x PBS (pH 7.4) and incubated with fresh BMDM media at 37 ^{o}C, 5% CO_2 for 24 hours. 24 hours post-infection, cultured supernatants were extracted for IL-23 ELISA (Biolegend 433704).

Statistical Analysis

All data was analyzed using FlowJo v10 (FlowJo, LCC) and/or Prism 10 (GraphPad Software). All graphs were analyzed using Mann-Whitney U-test. Significant values are symbolized with asterisks of * < 0.05, ** < 0.01, and ns for non-significant.

Results

Th17 induction during *M. tuberculosis* infection does not depend on duration or route of infection

We first tested whether the duration or route of infection has an impact on the generation of Th17 cells during Mtb infection. To test for induction of Th17 cells, we infected wild type mice with ~100 CFU of WT *M. tuberculosis* via the aerosol route, a standard dose for the mouse model (30). As previously published by multiple groups, we do not observe Th17 cells during the first month after Mtb infection of mice (19–22). At 4 weeks post-infection, we observed the expected plateau of CFU in the lungs of infected mice indicating the onset of T cell-based control of infection (Figure 1A). With stimulation using peptide pools from model antigens ESAT-6 and Antigen 85B (Ag85B) (31–33), we observed only IFN-γ$^+$ CD4$^+$ (Th1) T cells (Figure 1B) and no IL-17A$^+$ CD4$^+$ (Th17) T cells at this or earlier timepoints (Figure 1C). Th17 cells have been observed in humans, at times presumably long after initial infection (16–18). We therefore tested whether Th17 cells arise at late timepoints after infection in mice. Mice continued to have a Th1 response up to day 170 post-infection, with no increase in Th17 levels observed (Figures 1D-E). It was previously reported that infection with the virulent HN878 “Beijing” strain of the L2 lineage resulted in induction of Th17 cells (19). However, we did not observe a significant increase in IL-17A producing T cells in murine lungs when we infected with a Beijing strain at 3 weeks post-infection (Supplementary Figure S1).

The route of bacterial infection can impact which T helper cell types are induced. Infection via the intranasal route has been shown to elicit Th17 cells in response to infection with *Listeria monocytogenes* and Group A *Streptococcus* (12, 34). We therefore tested whether the intranasal route of infection results in a Th17 response in the lungs of Mtb infected mice. Mice were infected intranasally with ~100 CFU of WT Mtb into the lungs as measured on day 1 after infection. After four weeks of infection, mice infected by either route had comparable levels of bacteria in the lungs (Figure 1F). At this timepoint we again observed only IFN-γ producing CD4 T cells and very few IL-17A producing CD4 T cells in the lungs (Figures 1G-H). Thus, the route of infection with Mtb does not impact the dominant Th1-biased response observed during primary infection of naïve mice with Mtb. We next investigated whether exogenous IL-17A treatment provides protection against WT Mtb infection during primary infection. WT mice aerosol infected with WT Mtb were intranasally administered with either PBS control or 1 μg recombinant murine IL-17A daily between days 11 to 20 post-infection for a total of 10 doses (Figure 1I). WT mice intranasally (i.n.) administered 1 μg recombinant murine IL-17A daily were slightly more protected with ~3-fold reduction in lung CFU compared to WT mice given vehicle control. However, we observed no effect of IL-17A when it was administered via the intraperitoneal (i.p.) route. Cytokines are known to have short half-lives in vivo. Fusing a cytokine to serum albumin can increase its half-life, permitting greater efficacy (35). We therefore

fused IL-17A to murine serum albumin (MSA-IL-17A) and administered this construct either i.p. or i.n. at equimolar quantities compared to free IL-17A administered dosages. We found that i.n. delivery of this construct was more effective than delivery of IL-17A, with ~5-fold decrease in CFU observed in the lungs. In addition, fusion to albumin allowed us to observe efficacy with i.p. administration, resulting in a ~2-fold decrease in lung CFU. These results indicate that IL-17A can induce protective immunity to Mtb in the context of a primary infection, and that this may have potential as a therapeutic approach.

Tbet$^{-/-}$ mice are protected by a robust Th17 response during early *M. tuberculosis* infection

Because Th1 responses are known to inhibit Th17 responses (11, 13), we next tested whether Th1 differentiation masks a protective Th17 response during Mtb infection. *Tbx21*, also referred as Tbet, encodes the essential transcription factor that drives the Th1 lineage (11). Interestingly, *Tbet*$^{-/-}$ mice lack Th1 T cells but are not as susceptible to infection with Mtb as *Ifng*$^{-/-}$ mice (5, 36). As expected, we found that *Ifng*$^{-/-}$ mice were extremely susceptible to infection with Mtb, however *Tbet*$^{-/-}$ had CFU in the lungs equivalent to wild type mice at 21 days after infection (Figure 2A). Only WT mice had IFN-γ producing CD4 T cells in the lungs at this timepoint (Figures 2B, 2C). Importantly, *Tbet*$^{-/-}$ mice exhibited a robust population of IL-17A producing CD4 T cells at 3 weeks post-infection, confirming that Tbet prevents Th17 differentiation during Mtb infection (Figures 2B, 2D). Importantly, IFN-γ deficient mice did not exhibit elevated levels of IL-17A producing CD4 T cells demonstrating that IFN-γ production is not the mechanism by which Th1 T cells limit a Th17 response during Mtb infection (Figure 2D).

A previous study demonstrated that Tbet constrains effective T cell responses by promoting the differentiation of terminally differentiated non-protective intravascular Th1 T cells (37). This study also used antibody blockade of IL-17A in Tbet deficient mice to conclude that IL-17A provides minimal protection in this setting (37). However, given that antibody blockade is limited by its short duration and possibly incomplete inhibition, we tested whether genetically ablating IL-17A production in Tbet mice enhanced their susceptibility to Mtb infection. We therefore infected *Tbet*$^{-/-}$ and *Tbet*$^{-/-}$*Il17a*$^{-/-}$ (*Il17a*$^{icre/icre}$ referred to as *Il17a*$^{-/-}$) littermate-controlled mice with Mtb and measured CFU and T cell responses in the lungs after 3 weeks of infection. *Tbet*$^{-/-}$*Il17a*$^{-/-}$ mice were highly susceptible to Mtb infection with a 10-fold increase in lung CFU compared to WT and *Tbet*$^{-/-}$ mice, comparable to the susceptibility observed in *Ifng*$^{-/-}$ mice (Figure 2A). *Tbet*$^{-/-}$*Il17a*$^{-/-}$ mice completely lacked both IFN-γ producing (Figure 2C) and IL-17A producing CD4 T cells (Figure 2D). Notably, *Tbet*$^{-/-}$*Il17a*$^{-/-}$ mice still generated Th17 cells, as evidenced by the presence of the Th17 master transcription factor RORγT (11), despite their inability to produce IL-17A (Figures 2E, 2F). Together, these results indicate that IL-17A production by Th17 cells confers significant protection against Mtb infection in *Tbet*$^{-/-}$ mice, at least during early stages of infection.

M. tuberculosis utilizes ESX-1 and PDIM to limit Th17 response in mice

We next examined whether Mtb utilizes virulence factors to alter the host T helper response. The ESX-1 secretion system and the complex lipid PDIM are both known to influence production of cytokines known to impact Th17 differentiation (23, 24, 28, 38). Furthermore, these systems have been proposed to operate in the same virulence promoting pathway (28, 39). We therefore tested whether ESX-1 and PDIM might promote virulence in part by suppressing Th17 differentiation (Figure 3A). To test for a role of the ESX-1 secretion system, we infected mice with Δ*eccC1,* which lacks an ATPase required for ESX-1 function (ΔESX-1) (40) (Supplementary Figure S2A). We also utilized a mutant with an inactivating transposon insertion in *fadD28*, a gene required for PDIM biosynthesis (*fadD28::tn*, PDIM-lacking) (27) (Supplementary Figure S2B). As expected, ΔESX-1 and PDIM-lacking mutants were highly attenuated during infection at 3 weeks, exhibiting a 100-fold reduction in bacterial burden while complemented strains had similar CFU as WT Mtb (Supplementary Figure S3). Interestingly, ESAT-6 peptide pool stimulation of lung cells in ΔESX-1 and PDIM-lacking Mtb infected mice had an ~5-fold reduction in %IFN-γ$^+$ of CD4$^+$ T cells (Th1s) (Figure 3B) and ~2-fold increase in %IL-17A$^+$ of CD4$^+$ T cells (Th17s) (Figure 3C) compared to complemented strains of either mutant or WT Mtb. Similar results were seen with Ag85b peptide pool stimulation (Supplementary Figure S4A, S4B). To validate flow cytometry results we measured cytokine levels in lungs using BioLegend's LEGENDplex kit. We found that ΔESX-1 and PDIM-lacking mutants induced less IFN-γ (Figure 3D) while also inducing ~10x higher levels of IL-17A (Figure 3E) in the lungs compared with WT and complemented Mtb strains (Figures 3D-E). We tested if these elevated levels of Th17 cells and IL-17A contribute to the attenuation of ESX-1 and PDIM mutants by infecting littermate-controlled WT B6 and *Il17a*$^{-/-}$ mice with either WT, ΔESX-1, and complemented ΔESX-1 Mtb, or WT, PDIM-lacking, and complemented PDIM-lacking Mtb. Under the conditions where Th17s are highly induced, mice infected with either ΔESX-1 or PDIM-lacking Mtb, the *Il17a*$^{-/-}$ mice had ~3-5 fold higher CFU than WT mice (Figures 3F-G). These results indicate that the induction of Th17s is not dependent on the attenuation of Mtb in general, but instead Mtb utilizes ESX-1 and PDIM to suppress the induction of a Th17 response that enhances protection against Mtb infection.

To ensure that the increase in Th17s and IL-17A was not simply a consequence of infection with any attenuated Mtb mutant, we evaluated responses during infection with MmpL4 deficient (Δ*mmpL4*) bacteria. MmpL4 is a transmembrane transporter with proposed siderophore secretion activity (41) with no known association with the function of ESX-1 or secretion of PDIM (27). Δ*mmpL4* Mtb-infected mice had ~1.5 logs lower lung CFU than WT or complemented Mtb-infected mice (Figure 3H), a similar degree of attenuation as we observed with ESX-1 and PDIM mutants (Supplemental Figure S3). However, the Δ*mmpL4* Mtb-infected mice induced Th1 response that was indistinguishable from WT and complemented Mtb-infected mice (Supplemental Figure

S5) while not inducing greater numbers of Th17s compared to WT or complemented Mtb-infected mice (Figure 3I). Thus, the increase in Th17s we observed results from an ESX-1/PDIM specific mechanism.

Type I interferons boost Th1 induction and do not impact Th17 induction

As ESX-1 and PDIM are responsible for the host type I interferon response to Mtb infection (24, 28), and type I IFN is known to suppress Th17 responses (42), we investigated the impact of type I interferon signaling on Th17 induction during Mtb infection. We examined the effect of type I IFN both in WT B6 mice and in *Sp140*$^{-/-}$ mice that are highly susceptible to infection because of an excessive type I IFN response to infection (43). To abrogate type I IFN in each background we used mice deficient for the type I IFN receptor IFNAR. WT, *Ifnar1*$^{-/-}$, *Sp140*$^{-/-}$, *Sp140*$^{-/-}$*Ifnar1*$^{-/-}$, *Ifng*$^{-/-}$, and *Tbet*$^{-/-}$ mice were aerosol infected with WT Mtb. As expected, both *Sp140*$^{-/-}$ and *Ifng*$^{-/-}$ mice had up to 10-fold higher CFU than WT mice while *Ifnar1*$^{-/-}$, *Sp140*$^{-/-}$*Ifnar1*$^{-/-}$, and *Tbet*$^{-/-}$ mice were as resistant as WT mice at 3 weeks post-infection (Figure 4A). *Sp140*$^{-/-}$ mice had an almost 2-fold increase in %IFN-γ^{+} of CD4^{+} (Th1) T cells compared to WT mice, *Ifnar1*$^{-/-}$ had a 2-fold reduction in %IFN-γ^{+} of CD4^{+} (Th1) T cells compared to WT mice, *Sp140*$^{-/-}$*Ifnar1*$^{-/-}$ mice had a slightly stronger 4-fold reduction in %IFN-γ^{+} of CD4^{+} (Th1) T cells compared to *Sp140*$^{-/-}$ mice (Figures 4B-D). Importantly, deletion of IFNAR had no impact on Th17 induction in either WT or *Sp140*$^{-/-}$ mice, although we observed the expected increase in Th17 cells in Tbet deficient animals (Figure 4E). These results indicate that type I interferon signaling only impacts the induction of Th1s and does not influence Th17 induction, suggesting that induction of type I IFN by ESX-1/PDIM is not the mechanism by which these virulence factors suppress Th17 differentiation.

ESX-1 and PDIM alters conventional dendritic cell cytokine signaling in the mediastinal lymph node

Previous work suggested that ESX-1 mutants fail to suppress expression by macrophages of IL-12 p40, a subunit shared between IL-12 and IL-23 (24). Because IL-23 promotes Th17 responses, and ESX-1 and PDIM are responsible for the lack of a Th17 response during Mtb infection, we next investigated if ESX-1 and PDIM suppress IL-23 production in bone-marrow-derived macrophages (BMDMs) during in-vitro infection. ESX-1 and PDIM deficient strain both elicited a strong IL-23 response measured by IL-23 ELISA (Figure 5A). We then investigated if ESX-1 and PDIM suppress IL-23 production by dendritic cells during in vivo infection in the draining (mediastinal) lymph nodes. We infected mice with ~100 CFU via the aerosol route and harvested mediastinal lymph nodes at 21 days post-infection. We examined IL-12 and IL-23 production by conventional dendritic cells using ICS. To clearly distinguish between levels of these two cytokines we used ICS for the cytokine specific subunits: IL-12 p35 and IL-23 p19. First, we found that type 1 conventional dendritic cells (cDC1s), known to be specialized for IL-12 production,

produce robust levels of IL-12 p35 during infection with WT Mtb (Figures 5B, 5C). However, both ESX-1 and PDIM deficient strains elicited significantly lower levels of IL-12 p35 from these cells (Figures 5B, 5C), consistent with the lower bacterial burdens in the lungs of mice infected with these mutants (Supplementary Figure S3). During infection with wild-type bacteria, we observed very little IL-23 p19 production by type 2 conventional dendritic cells (cDC2s) in the draining mediastinal lymph node (Figures 5D, 5E). Importantly, ESX-1 and PDIM-lacking Mtb infection resulted in an increase in the percentage of cDC2s that produce IL-23 p19 in mediastinal LNs (Figures 5D, 5E). We saw very little to no IL-23 p19 expression in cDC1s and IL-12 p35 expression in cDC2s with no differences between WT or ESX-1 and PDIM deficient strains (Supplementary Figure S6). These results indicate that the ESX-1 and PDIM virulence factors impact naïve T cell differentiation at the draining mediastinal lymph node by promoting IL-12, a Th1-polarizing cytokine, and limiting IL-23, a Th17-polarizing cytokine, expression in cDC1s and cDC2s respectively.

Discussion

The rise of multidrug-resistant and extensively drug-resistant strains, combined with a limited pipeline of new drugs, underscores the urgent need for effective vaccines. Achieving the World Health Organization/STOP TB Partnership's target of TB elimination by 2050 will not be possible without a highly efficacious vaccine (44). Unlike most successful vaccines, which protect through neutralizing antibodies, TB immunity primarily depends on T-cell–mediated responses, for which no clear vaccine strategy exists. Defining protective immune mechanisms is therefore critical—not only for guiding vaccine design but also for advancing immune-based therapies. Equally important is understanding how *M. tuberculosis* evades or suppresses these responses, as such insights can inform both vaccine development and therapeutic interventions.

We sought to understand why Mtb infection does not elicit Th17 production robustly during primary infection. We found that this is independent of duration and route of infection but instead results from an overly robust Th1 response, which suppresses Th17 development, and upon the virulence factors ESX-1 and PDIM. It has been long established that Th1 cells are important for control of Mtb infection, yet there have also been hints in the literature that Th1 cells are not simply protective. First, excessive IFN-γ production is harmful, driving tissue destruction in the lungs (45), which may benefit bacteria by promoting necrosis and transmission. Interestingly, the majority of T cell antigens are highly conserved across Mtb (46), suggesting that dominant Th1 cell responses may confer some benefit to Mtb. Indeed, a recent study suggested that while common antigens are likely to drive Th1 differentiation, rare variable antigens are more likely to drive Th17 differentiation in Mtb infected patients (47). Thus, it is feasible that Mtb promotes excessive Th1 differentiation in part to prevent potentially protective Th17 cells from emerging.

Given that ESX-1 and PDIM mutants elicit type I IFN, and type I IFN suppresses Th17 cells, it is perhaps surprising that type I IFN does not explain the suppression of Th17 we observe during early infection. Type I IFN is clearly detrimental to Mtb infection, as deletion of IFNAR rescues the susceptibility of mice that exhibit type I IFN driven disease (24, 43). However, type I IFN is known to have many immunosuppressive functions that could explain its detrimental role in Mtb infection (48). Many cytokines are known to participate in the differentiation of Th17 cells including TGF-β, IL-6 and IL-23. Importantly, IL-23 is essential for maintaining the Th17 lineage, while TGF-β and IL-6 are critical for its induction. The crucial role of IL-23 differentiation and maintenance of Th17 cells in vivo is well established (49, 50). IL-23 supports IL-17 production by upregulating IL-17 itself, RORγt and other pro-inflammatory cytokines (51). Our in vivo data demonstrating increased IL-23 production by dendritic cells in ESX-1 mutant infections is consistent with the old observation that ESX-1 suppresses IL-12 p40 in vitro. Future work will focus on elucidating the mechanism of Mtb suppression of IL-23. In addition, the work

in this study adds to the growing evidence that ESX-1 and PDIM are phenotypically linked. Unlike what has been demonstrated in the H37Rv strain (28), we do not find that PDIM mutants have a defect in ESX-1 function or that ESX-1 mutants have any changes in PDIM production or secretion. This could be a strain specific difference, especially as it is known that H37Rv has a unique point mutation that causes downregulated ESX-1 function relative to Erdman and most clinical strains (52). In the future, it will be important to establish how ESX-1 and PDIM functions are linked. Secretion of the ESX-1 substrate ESAT-6 is generally used as a proxy for ESX-1 function. It is possible that PDIM loss has more subtle effects on ESX-1 function that are not reflected by ESAT-6 secretion levels.

Because primary infection does not reliably elicit Th17 T cells, it has been difficult to study the function of these cells. A method for reliably inducing Th17s in mice during infection would facilitate studying the role of Th17-mediated protection. We show here that mice lacking Tbet respond to WT Mtb infection with a Th17 response and provide protection mediated by IL-17A during early infection. Thus, *Tbet*$^{-/-}$ mice can be used to interrogate mechanisms underlying Th17 mediated protection during primary Mtb infection. High Th17 plasticity permits Th17s to express a wide variety of T helper subset profiles that can range from pro-inflammatory Th17.1s that co-express IFN-γ and IL-17A to anti-inflammatory Tr1-like Th17s that co-express IL-10 and IL-17A (53). Moving forward, it will be important to delineate in depth which Th17 subsets and which mechanisms downstream of IL-17 receptor signaling are important for controlling Mtb infection. Importantly, we show that exogenous administration of recombinant IL-17A leads to a decrease in CFU in Mtb infected lungs by up to ~5x. Our data suggests that a limiting factor for efficacy of recombinant IL-17A is its short half-life. Future efforts focused on methods for improving the stability of this cytokine in vivo could lead to more dramatic reductions in bacterial burdens.

The live vaccine strain Bacille Calmette-Guerin (BCG) was developed by extensive laboratory passage of *Mycobacterium bovis*, resulting in attenuation of virulence (54, 55). This attenuation makes BCG a very safe vaccine. However, although BCG is effective in preventing severe tuberculosis in children, it is not sufficiently effective against adult pulmonary tuberculosis to make a significant impact on TB cases worldwide. A cause of the reduced virulence of BCG is the loss of multiple genes associated with the ESX-1 type VII secretion system. To create a live vaccine that is safe yet more effective than BCG, scientists engineered MTBVAC, a vaccine candidate currently in phase 2b trials. Unlike BCG, MTBVAC is derived from Mtb. MTBVAC is attenuated by mutation of the ESX-1 secretion system and a mutation that eliminates PDIM (56). Our insights into how ESX-1 and PDIM suppress effective immune responses could promote understanding of how MTBVAC provides protective immunity. Indeed, MTBVAC has been demonstrated to elicit mucosal-homing-marker expressing Th17s ideal for better control of Mtb infection (57). In addition, understanding the role and function of Th17 cells more generally can help promote development of the next generation of effective Mtb vaccine candidates.

Acknowledgements
We thank Russell Vance's lab for the kind gifts of *Sp140*$^{-/-}$, *Ifnar1*$^{-/-}$, and *Sp140*$^{-/-}$*Ifnar1*$^{-/-}$ mice. We thank Jeff Cox's lab for the kind gifts of ΔESX-1 (Δ*eccC1*), complemented ΔESX-1, PDIM-lacking (Δ*fadD28*), complemented PDIM-lacking, ΔMmpL4 (Δ*mmpL4*), and complemented MmpL4 Mtb Erdman strains. We thank Helia Samani, Scott Espich, Vicky Wu, Malia Wilson, and Cielo Kwon for assistance in mouse colony maintenance. We thank members of the Stanley, Cox, and Vance laboratories for helpful discussions. Funding was from NIH P01 AI063302 Project 4 to SAS and NIH 1R01AI113270-01A1 to SAS.

Figures

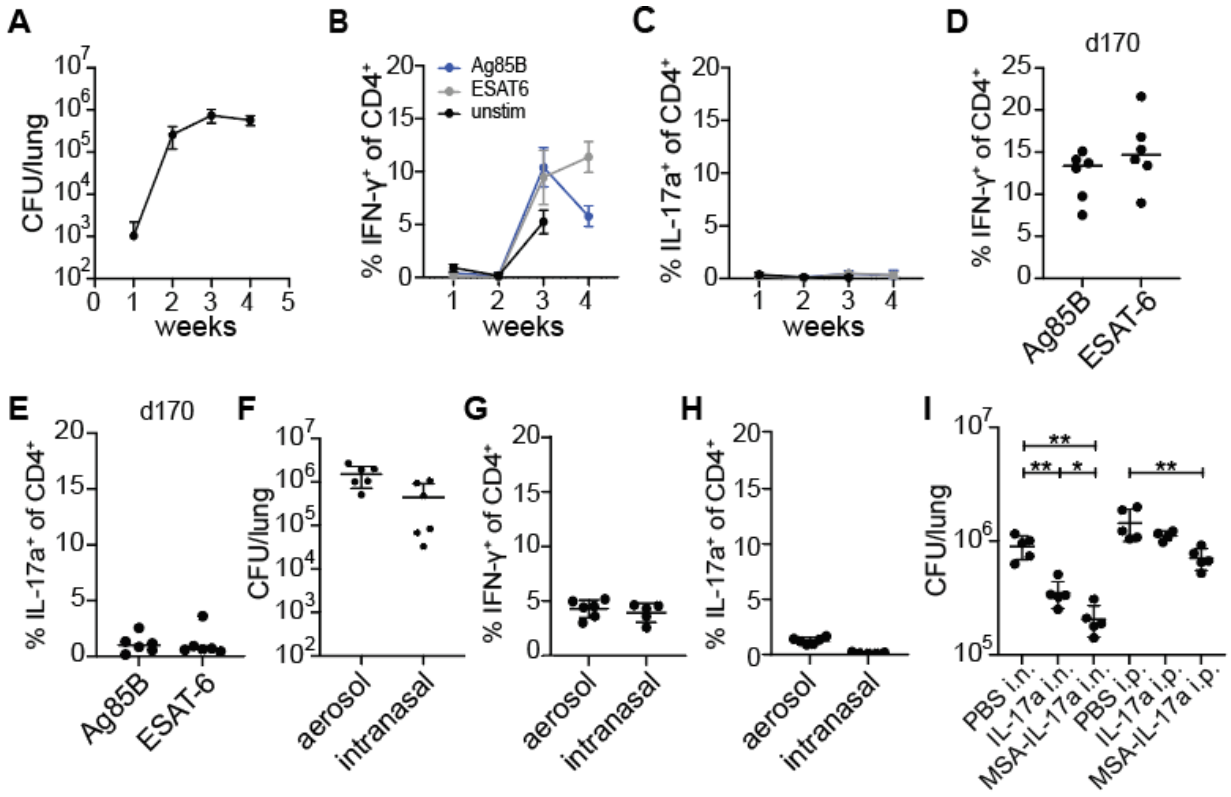

Figure 1. Lack of Th17 induction during WT *M. tuberculosis* infection is not due to duration or route of infection. (A-C) WT B6 mice were aerosol infected with WT *M. tuberculosis* Erdman strain and lungs were evaluated at 21 days post-infection (dpi) for **(A)** bacterial burdens by CFU **(B)** IFN-γ$^+$ CD4$^+$ T cells and **(C)** IL-17A$^+$ CD4$^+$ T cells using flow cytometry. Cytokines were measured using ICS after restimulation with Ag85b or ESAT-6 peptide pools. **(D-E)** Mice were infected and analyzed at 170 dpi for **(D)** IFN-γ$^+$ CD4$^+$ T cells and **(E)** IL-17A$^+$ CD4$^+$ T cells in lungs. **(F-H)** WT B6 mice were either aerosol infected or intranasally infected with WT *M. tuberculosis* Erdman strain and evaluated 28 dpi for **(F)** bacterial burdens in lungs by CFU, **(G)** IFN-γ$^+$ CD4$^+$ T cells and **(H)** IL-17A$^+$ CD4$^+$ T cells in lungs by flow cytometry. Cytokines were measured using ICS after restimulation with ESAT-6 peptide pool. **(I)** WT B6 mice were aerosol infected with WT *M. tuberculosis* and treated with PBS control, recombinant murine IL-17A (IL-17A) or recombinant murine IL-17A fused to murine serum albumin (MSA-IL-17A) daily either using the intranasal (i.n.) or intraperitoneal (i.p.) routes between days 11 to 20 post-infection. CFU in lungs was measured at 21 dpi. Results are representative of at least 2 biological replicates. For all graphs, each dot represents an individual mouse. *p<0.05, **p<0.01 (unpaired nonparametric Mann-Whitney U test).

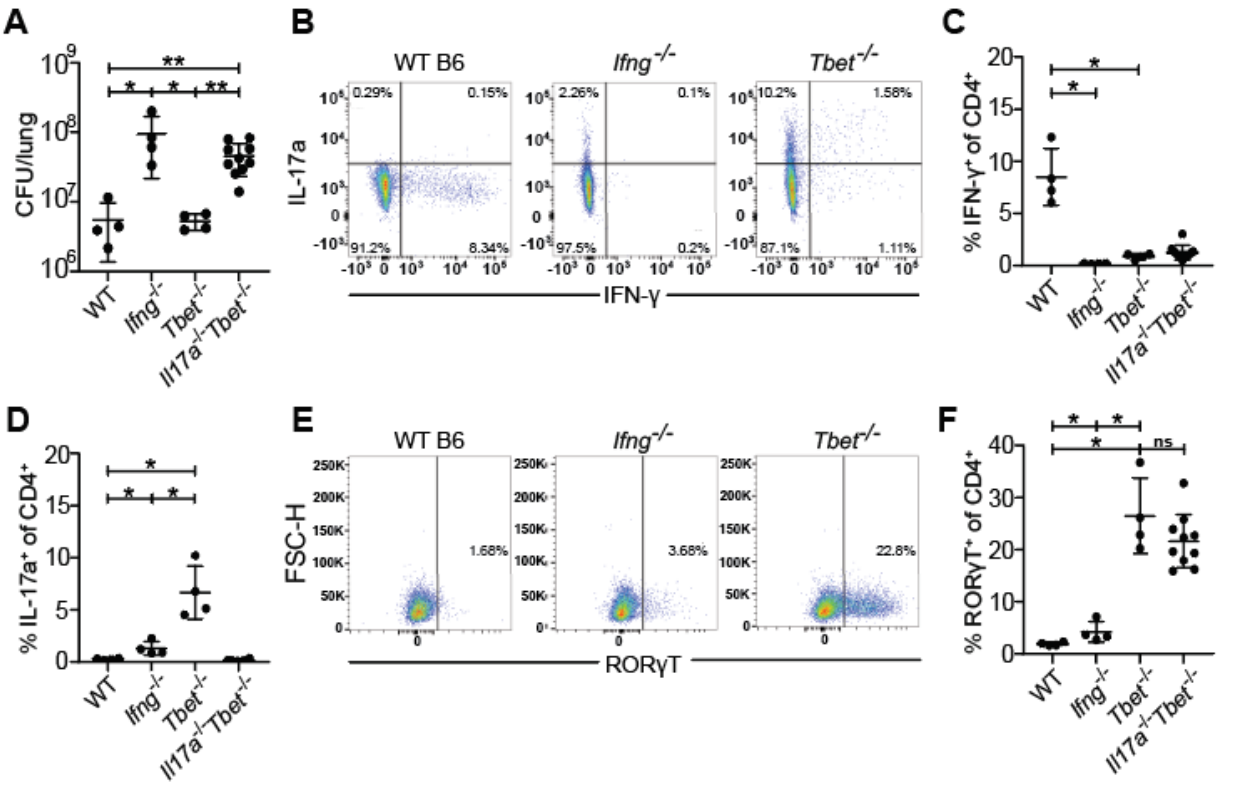

Figure 2. *Tbet*$^{-/-}$ mice are protected from susceptibility to Mtb infection by the emergence of Th17 cells. WT B6, *Ifng*$^{-/-}$, *Tbet*$^{-/-}$, and *Il17a*$^{-/-}$*Tbet*$^{-/-}$ mice were aerosol infected with WT *M. tuberculosis* Erdman strain. *Tbet*$^{-/-}$ and *Il17a*$^{-/-}$*Tbet*$^{-/-}$ mice were littermate-controlled. Mice were infected with Mtb and evaluated 21 days post-infection for **(A)** CFU in the lungs of indicated genotypes or **(B-F)** cellular immune responses using flow cytometry. CD4$^+$ T cells were gated on single, live, MHC-II$^-$, Ly6G$^-$, CD3$^+$, γδTCR$^-$, CD4$^+$, CD8a$^-$ cells for analysis of IFN-γ **(B,C)**, IL-17 **(B,D)** and RORγT **(E,F)**. Results in A-F are representative of 3 independent experiments. *, $p < 0.05$; **, $p < 0.01$ (unpaired nonparametric Mann-Whitney U test).

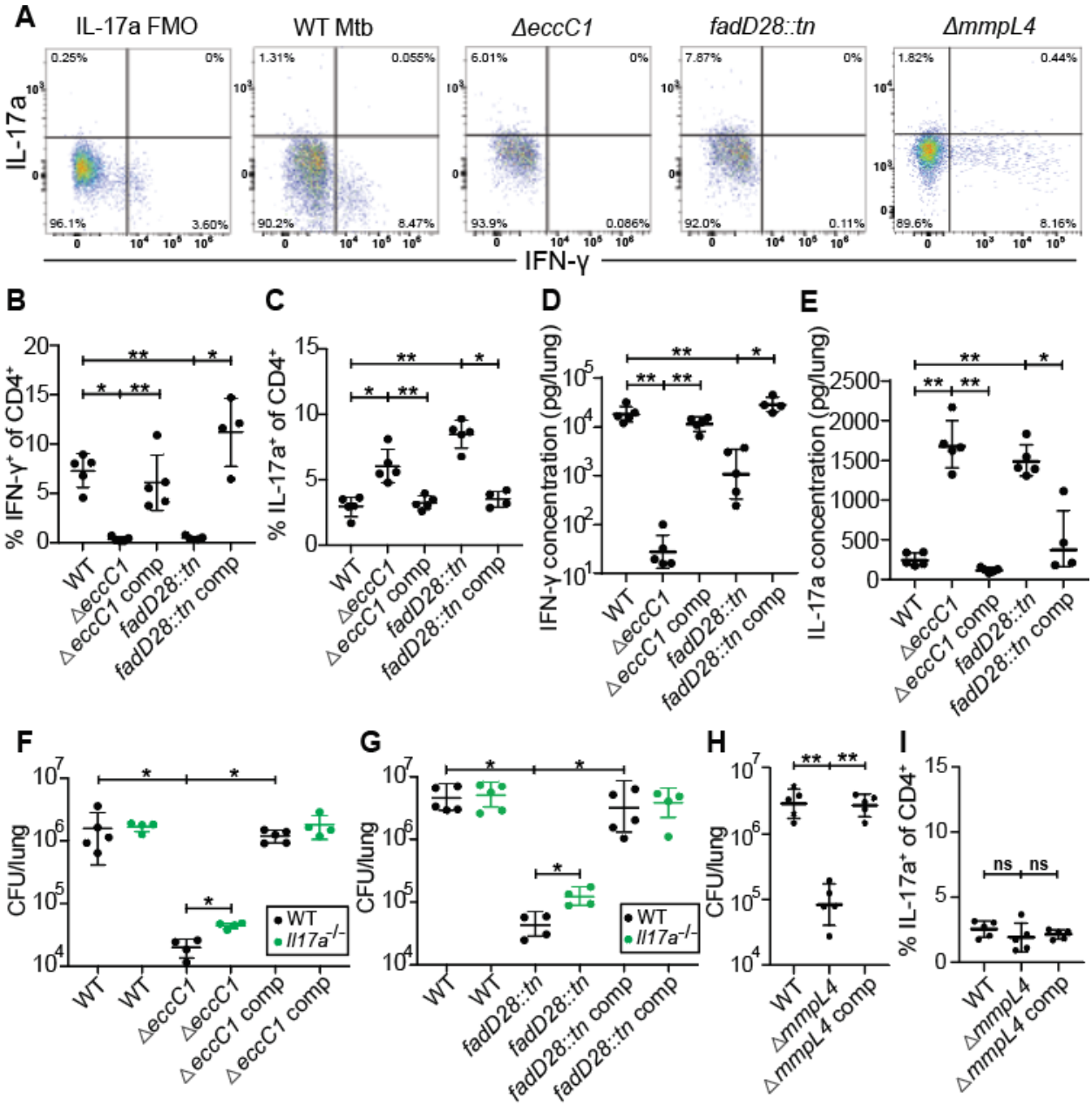

Figure 3. *M. tuberculosis* ESX-1 and PDIM virulence factors suppress Th17 response in mice. WT B6 mice were aerosol infected with indicated strains and evaluated at 21 days post-infection. **(A)** Representative flow cytometry plots (cells gated on single, live, MHC-II$^-$, Ly6G$^-$, CD3$^+$, γδTCR$^-$, CD4$^+$, CD8a$^-$) of IFN-γ$^+$ and IL-17A$^+$ CD4$^+$ T cell populations. Mice were sacrificed and evaluated with ESAT-6 peptide pool stimulated lung homogenates for **(B)** IFN-γ$^+$ CD4$^+$ T cells and **(C)** IL-17A$^+$ CD4$^+$ T cells by flow cytometry. Mice were sacrificed and lung homogenates were evaluated with BioLegend LEGENDplex for **(D)** IFN-γ and **(E)** IL-17A protein concentrations. **(F-G)** Littermate-controlled WT B6 and *Il17a*$^{-/-}$ mice were aerosol infected with indicated strains and sacrificed at 21 days post-infection with lung homogenate plated for CFU. **(H-I)** Mice were infected with WT, *mmpl4* mutant, or complemented *mmpl4* mutant Mtb

and evaluated for **(H)** day 21 CFU and **(I)** IL-17A$^+$ CD4$^+$ T cells by flow cytometry. Results are representative of 2 independent experiments. *, $p < 0.05$; **, $p < 0.01$ (Mann-Whitney U test).

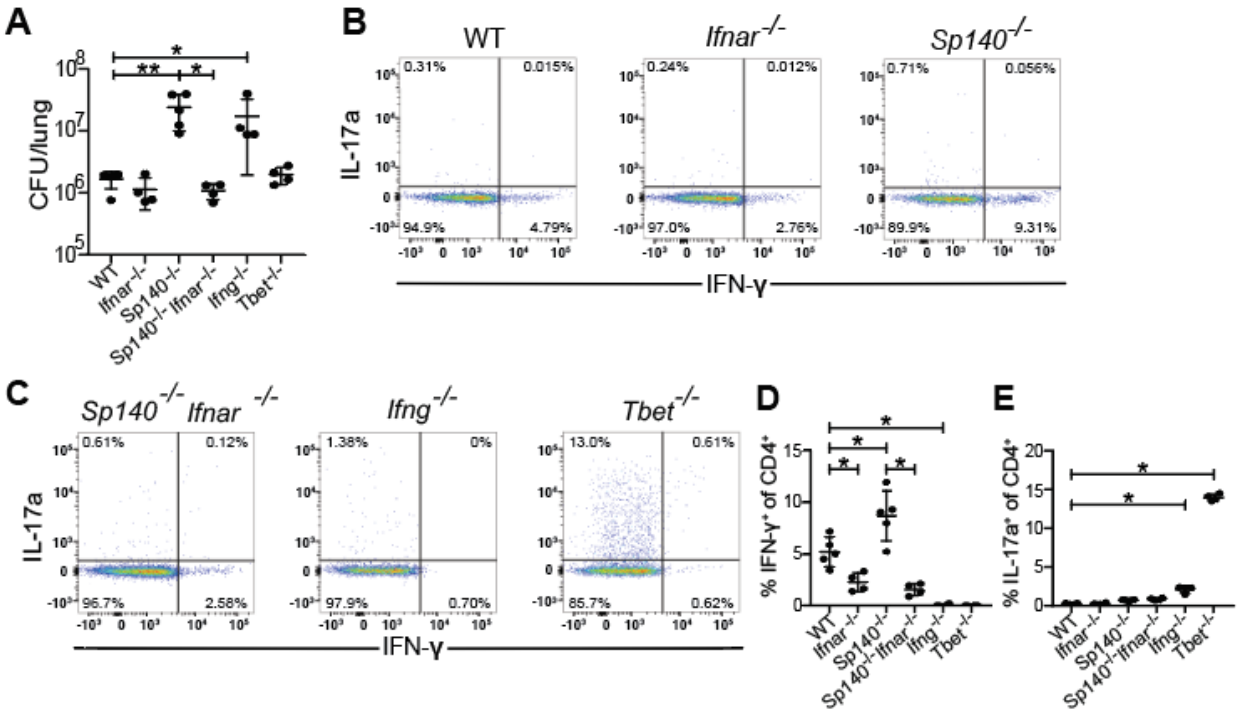

Figure 4. Type I interferon signaling boosts Th1 induction and does not impact Th17 induction. WT B6, *Ifnar*$^{-/-}$, *Sp140*$^{-/-}$, *Sp140*$^{-/-}$*Ifnar*$^{-/-}$, *Ifng*$^{-/-}$, and *Tbet*$^{-/-}$ mice were aerosol infected with WT *M. tuberculosis* Erdman strain. **(B, C)** Representative flow cytometry plots (cells gated on single, live, MHC-II^{-}, Ly6G^{-}, CD3^{+}, γδTCR^{-}, CD4^{+}, CD8a^{-}) of IFN-γ^{+} and IL-17A^{+} CD4^{+} T cells of these populations. 21 days post-infection, lung homogenates were measured for **(A)** CFU and analyzed via flow cytometry for **(D)** IFN-γ^{+} CD4^{+} T cells and **(E)** IL-17A^{+} CD4^{+} T cells. Results in A, D, and E are representative of 2 independent experiments. *, $p < 0.05$; **, $p < 0.01$ (unpaired nonparametric Mann-Whitney U test).

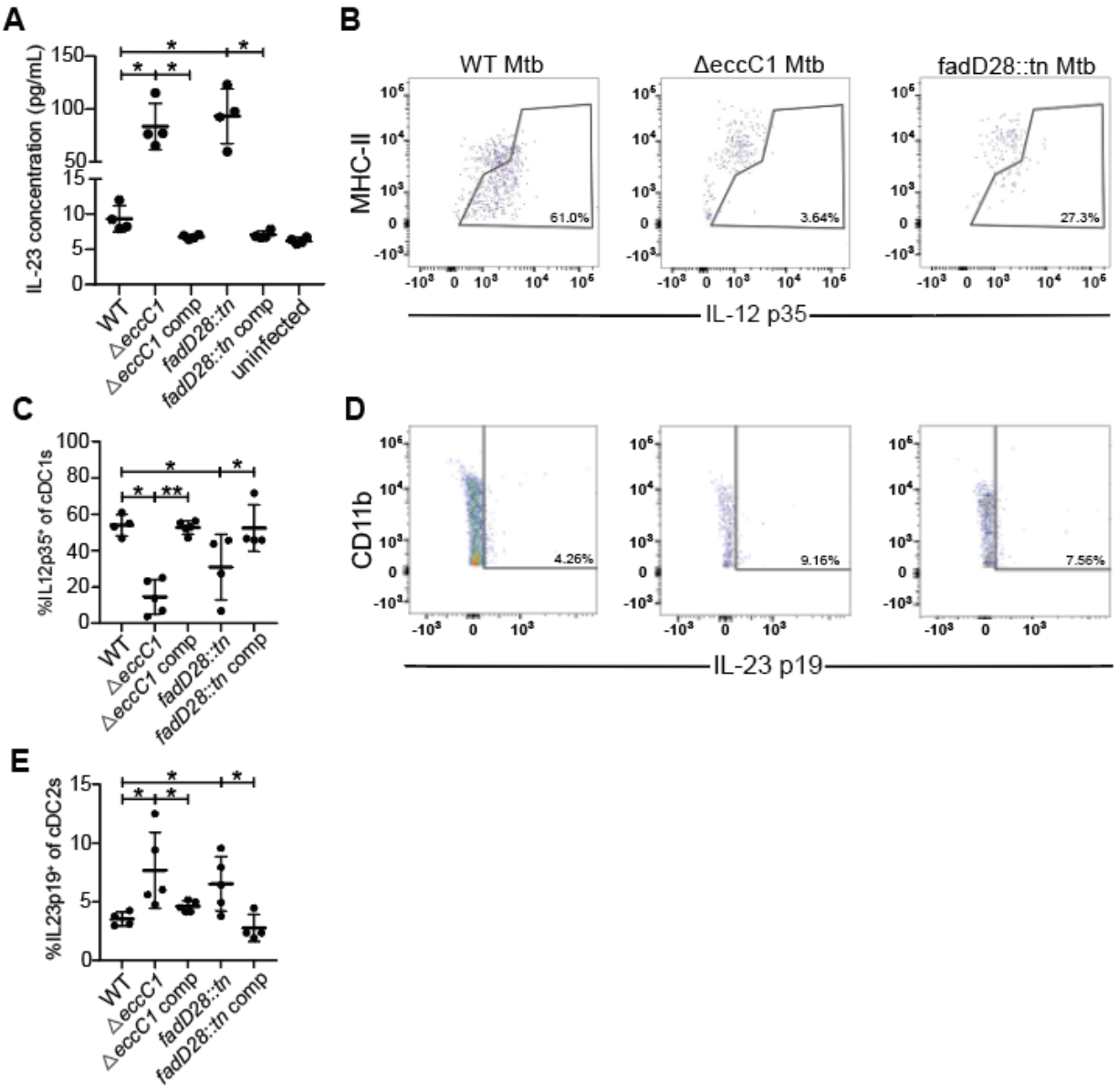

Figure 5. ESX-1 and PDIM alter conventional dendritic cell cytokine signaling in the mediastinal lymph node. WT B6 bone-marrow-derived macrophages were infected with designated Mtb Erdman strains at MOI = 10 or uninfected for 24 hours with **(A)** IL-23 ELISA taken from cultured supernatants. WT B6 mice were aerosol infected with indicated strains and analyzed at 21 days post-infection **(C,E)** Flow cytometry schematic for gating of **(B)** cDC1 (gated on single, live, $CD3^{-}$, $CD19^{-}$, $CD11c^{+}$, $MHC\text{-}II^{+}$, $XCR1^{+}$, $CD11b^{-}$) and **(D)** cDC2 (gated on single, live, $CD3^{-}$, $CD19^{-}$, $CD11c^{+}$, $MHC\text{-}II^{+}$, $XCR1^{-}$, $CD11b^{+}$) populations of mediastinal lymph nodes with representative flow cytometry plots of IL-12 $p35^{+}$ and IL-23 $p19^{+}$ gating of cDC1 and cDC2 populations respectively. 21 days post-infection, mediastinal lymph nodes from WT B6 mice were aerosol infected with either WT, ΔeccC1 (ΔESX-1), complemented ΔeccC1::eccC1, transposon-inserted fadD28::tn (PDIM-lacking),or complemented transposon-inserted

fadD28::tn + pfadD28 *M. tuberculosis* Erdman strain were extracted and analyzed for IL-12 $p35^+$ cDC1s **(C)** and IL-23 $p19^+$ cDC2s **(E)** by flow cytometry. Results in A, C, and E are representative of 2 independent experiments. *, $p < 0.05$; **, $p < 0.01$ (unpaired nonparametric Mann-Whitney U test).

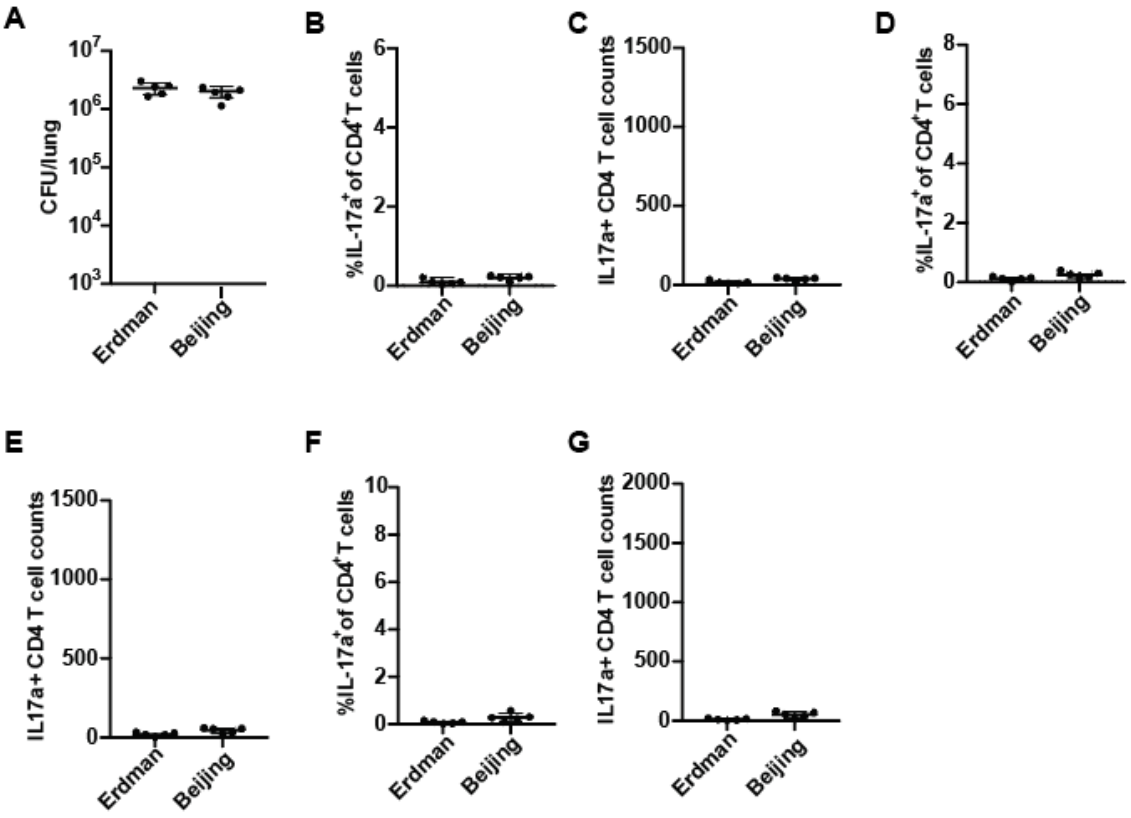

Figure S1. *M. tuberculosis* strains Erdman and Beijing both only induce Th1s. Mice were infected with either the Erdman or Beijing strain of Mtb via the aerosol route and evaluated at 21dpi for **(A)** CFU in the lungs or **(B-G)** IL-17A$^+$ CD4$^+$ T cells in the lungs. **(B,C)** unstimulated, **(D,E)** restimulated with Antigen 85B peptide, **(F,G)** restimulated with ESAT-6 peptide. Representative experiment of 2.

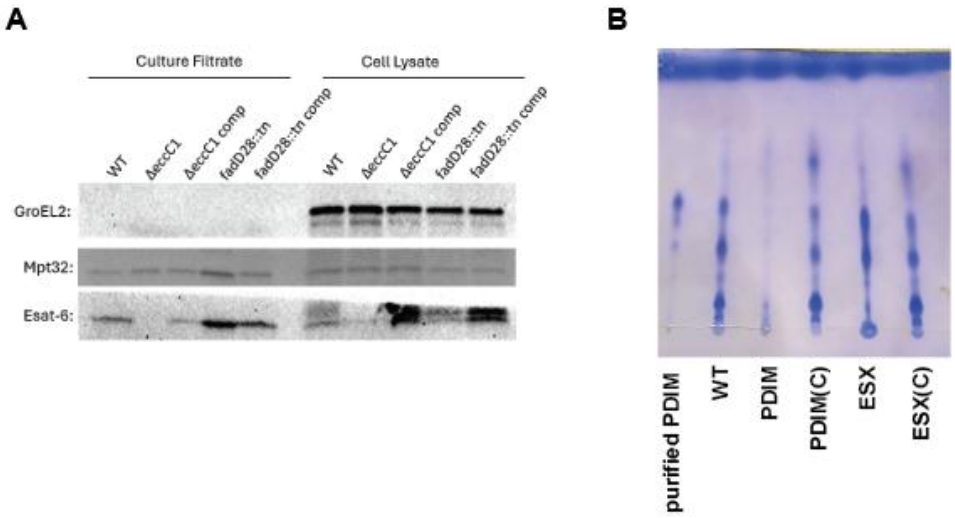

Figure S2: Mtb Erdman PDIM mutants secrete ESAT-6 and ESX-1 mutants produce PDIM. (A) WT, Δ*eccC1*, complemented Δ*eccC1::eccC1* (Δ*eccC1* comp), *fadD28::tn*, or *fadD28::tn* + p*fadD28* (fadD28::tn comp) *M. tuberculosis* Erdman strain were cultured in Sauton's complete media without Tween-80 for 5 days. Cell lysate and culture supernatant were processed through SDS-PAGE and Western blot analysis. Anti-ESAT-6 antibody was used for detecting ESAT-6. Anti-Mtb GroEL2 antibody (BEI Resources NR-13657) was used as a loading control for the cell lysate fraction. Anti-Mtb Mpt32 antibody (BEI Resources NR-13807) was used as a loading control for the culture filtrate. Results shown are from 1 experiment representative of 2 independent experiments. **(B)** WT, Δ*eccC1* (ESX), complemented Δ*eccC1::eccC1* (ESX(C), *fadD28::tn* (PDIM), or *fadD28::tn* + p*fadD28* (PDIM(C)) *M. tuberculosis* Erdman strain were cultured in 7H9 media. Outer leaflet of mycomembrane was removed via hexanes wash, concentrated and separated on TLC plate with 98:2 petroleum ether:acetone mobile phase. TLC plate was stained with 0.2% Coomassie blue in 20% methanol. Results shown are from 1 experiment representative of 2 independent experiments.

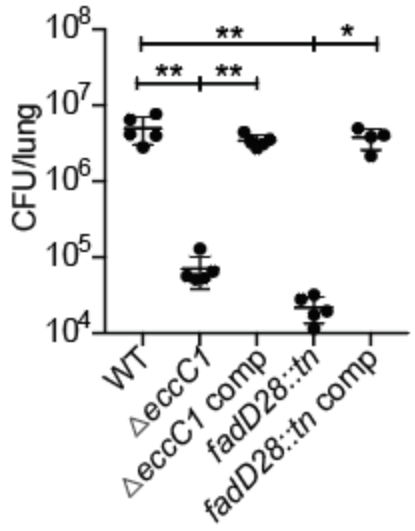

Figure S3. Attenuation of ESX-1 and PDIM mutants at 21 days post-infection. WT B6 mice were aerosol infected with either WT, Δ*eccC1,* Δ*eccC1::eccC1*, *fadD28::tn*, or *fadD28::tn* + p*fadD28 M. tuberculosis* Erdman strain. 21 days post-infection, mice were sacrificed, and CFU were enumerated from lung lysates.

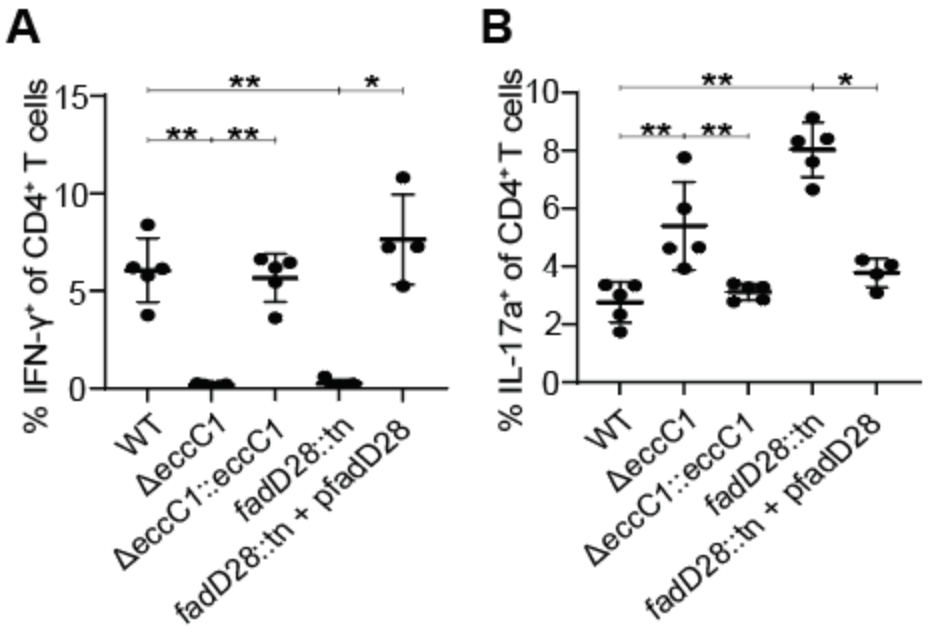

Figure S4: Antigen 85b stim resembles ESAT-6 stimulation for IFN-γ and IL-17A staining of CD4⁺ T cells. As in Figure 3, WT B6 mice were aerosol infected with either WT, Δ*eccC1,* Δ*eccC1::eccC1*, *fadD28::tn*, or *fadD28::tn* + p*fadD28 M. tuberculosis* Erdman strain. 21 days post-infection, mice were sacrificed, lung single cell homogenates were stimulated with Antigen 85b peptide pool and measured for lung **(A)** IFN-γ⁺ CD4⁺ T cells and **(B)** IL-17A⁺ CD4⁺ T cells by flow cytometry. Results in A and B are representative of 2 independent experiments. *, $p < 0.05$; **, $p < 0.01$ (unpaired nonparametric Mann-Whitney U test).

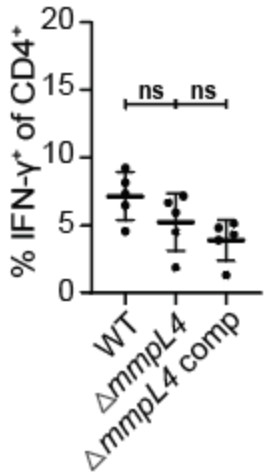

Figure S5: Δ*mmpL4* Mtb induces similar IFN-γ⁺ CD4⁺ T cells as WT or complemented Mtb. Mice were aerosol infected with WT, Δ*mmpL4* mutant, or complemented Δ*mmpL4* Mtb Erdman strain and evaluated for IFN-γ⁺ CD4⁺ T cells after restimulation with ESAT-6 peptide by flow cytometry. Results are representative of 2 independent experiments. *, $p < 0.05$; **, $p < 0.01$ (unpaired nonparametric Mann-Whitney U test).

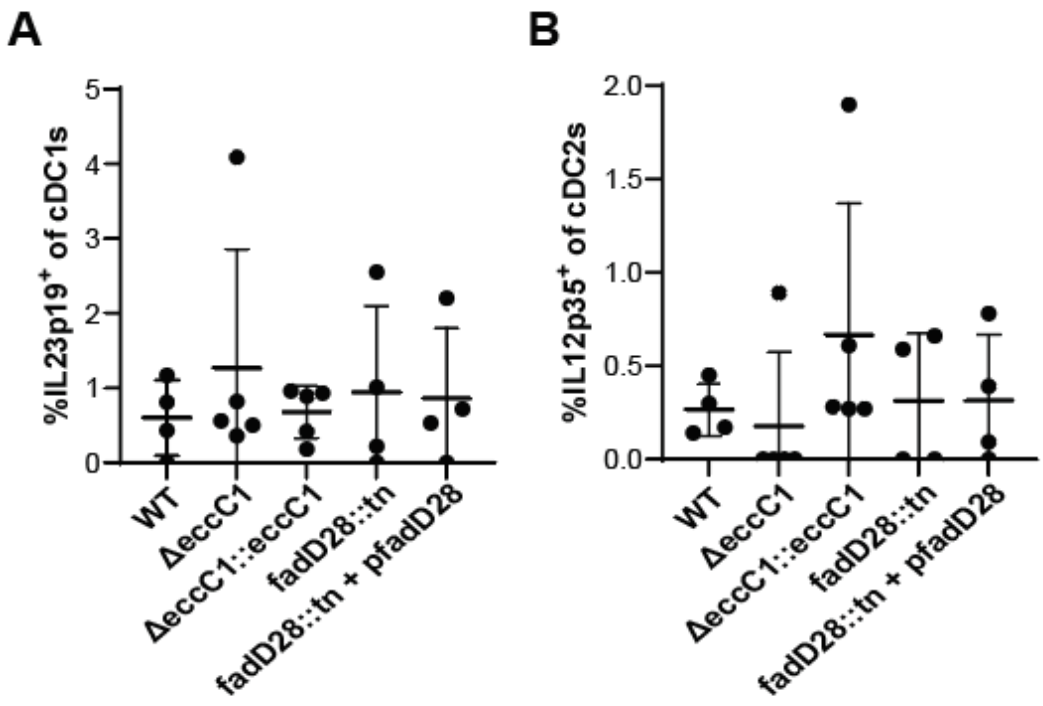

Figure S6: There is little to no IL-23 p19 expression in cDC1s and IL-12 p35 expression in cDC2s during Mtb infection. As in Figure 5, WT B6 mice were aerosol infected with WT, Δ*eccC1,* Δ*eccC1::eccC1*, *fadD28::tn*, or *fadD28::tn* + p*fadD28 M. tuberculosis* Erdman strain. 21 days post-infection, mice were sacrificed, mediastinal lymph nodes were extracted and processed for ICS. Analysis of **(A)** IL-23 p19^{+} cDC1s and **(B)** IL-12 p35^{+} cDC2s by flow cytometry. Results in A and B are representative of 2 independent experiments. (unpaired nonparametric Mann-Whitney U test).

Chapter Two: An operon encoding two secreted nucleases mediates virulence in Methicillin-resistant *Staphylococcus aureus*

This work is currently unpublished and has not been uploaded to BioRxiv yet:

Alex Zilinskas, Heyuan Michael Ni, Zoe Netter, Kuei-Ho Chen, Danielle L. Swaney, Amir Balakhmet, Nevan Krogan, Sarah Stanley

Abstract

Methicillin-resistant *Staphylococcus aureus* (MRSA) is an opportunistic pathogen that colonizes a significant proportion of humans, contains numerous virulence factors promoting infection, and continues to threaten human lives and burden healthcare systems globally. Many MRSA virulence factors are known to be either secreted or anchored on the outer leaflet of the cell surface. Although many virulence factors have been studied intensively in MRSA, there remains a significant proportion of secreted and surface proteins that remain unstudied for potential as virulence factors. We began with identifying proteins secreted from MRSA in axenic culture using an unbiased mass-spectrometry based approach. 2 secreted proteins thus identified mapped to an operon of 6 genes, *SAUSA300_1739* to *SAUSA300_1744*. Mutation of each of the individual genes in the operon resulted in attenuation in a mouse model of subcutaneous infection. We demonstrate that two genes in the operon, *SAUSA300_1739*, and *SAUSA300_1740,* encode nucleases with DNase activity. Genetic analysis of the *SAUSA300_1739* to *SAUSA300_1744* operon across several *Staphylococcus aureus* strains indicate that the operon is highly conserved, highlighting its importance for virulence.

Introduction

Staphylococcus aureus is an opportunistic pathogen which colonizes approximately 30-50% of healthy humans (58, 59). *S. aureus* belongs to the “ESKAPE” group of pathogenic bacteria known for their ability to spread in modern hospital care settings and increases in antimicrobial resistant infections (60). In 2017, the more pathogenic and antimicrobial-resistant version of *S. aureus*, Methicillin-resistant *Staphylococcus aureus* (MRSA), caused approximately 300,000 hospitalizations, 10,000 deaths, and $1.7 billion in healthcare costs in the United States alone (61). In 2019, MRSA was estimated to cause up to 120,000 deaths worldwide (60). Although MRSA infections can manifest in different tissues, it primarily causes skin and soft tissue infections (SSTIs) with incidence rates of 32.1 to 48.1 per 1,000 (62). The dominant MRSA clonal type in North America is USA300, which accounts for a large proportion of community- and hospital-acquired infections (63).

The global success of *S. aureus* in causing high morbidity and mortality is largely attributable to its arsenal of virulence factors. These virulence factors promote immunoevasion, induce host cell lysis, induce non-specific T cell receptor activation, prevent antibody and complement-mediated antimicrobial functions, breakdown antibacterial compounds including reactive oxygen species, and inhibit chemotaxis (64). One virulence strategy used by *S. aureus* is the deployment of secreted nucleases. *S. aureus* is known to secrete Nuc1 and have surface-bound Nuc2 DNA nucleases (65), and secrete the EssD DNA nuclease (66) to form biofilms and degrade neutrophil extracellular traps (NETs) to promote infection.

Despite the characterization of many virulence factors, a large percentage of genes in the *S. aureus* pangenome remain unannotated or limited to predicted function. With many genes with unknown or poorly annotated functions, this suggests that our inventory of *S. aureus* virulence factors remains incomplete. Uncovering these hidden factors and understanding their impacts on the host is necessary to promote novel vaccine and therapeutic development.

Because a large proportion of *S. aureus* virulence factors are secreted or surface-anchored, we focused on characterizing a secreted proteome of the North America-dominant MRSA USA300 clonal type in defined media, including under acidic conditions and hydrogen peroxide stress. We identified a total of 109 secreted proteins, 29 of which have unknown protein function and have not been studied for role in *S. aureus* virulence. Using this dataset, we identified 21 transposon mutants, available in a non-essential gene arrayed transposon library, with loss of function mutations in genes without established function and assayed them for virulence defects. We found that two genes, *SAUSA300_1739* and *SAUSA300_1740* are dispensable for growth in liquid culture, however are required for full virulence in a murine subcutaneous infection model. Furthermore, we demonstrate that both SAUSA300_1739 and SAUSA300_1740 are nucleases with DNase activity. Finally, we show that every gene in the six gene operon

encoding SAUSA300_1739 and SAUSA300_1740 contributes to the virulence of MRSA. We find that this operon is highly conserved across MRSA strains, underscoring its importance for virulence.

Materials and Methods

Ethics statement

All procedures involved with the use of mice were approved by the University of California, Berkeley's Institutional Animal Care and Use Committee (protocol 2015-09-7979). All protocols conform to federal regulations, the National Research Council Guide for the Care and Use of Laboratory Animals, and the Public Health Service Policy on Humane Care and Use of Laboratory Animals.

Bacterial culture for mass spectrometry

Minimal media at pH 7.4 was inoculated with WT Methicillin-resistant *Staphylococcus aureus* USA300 strain SF8300 and grown overnight at 37 ^{o}C, 180 rpm. Media was prepared with (mg/mL): K_2HPO_4 (70), KH_2PO_4 (20), and $(NH_4)_2SO_4$ (10), along with the amino acids phenylalanine (4), isoleucine (3), tyrosine (5), cysteine (2), glutamate (10), lysine (1), methionine (7), histidine (3), tryptophan (1), leucine (9), aspartate (9), arginine (7), serine (3), alanine (6), threonine (3), glycine (5), valine (8), and proline (1). It also included the nucleobases adenine (0.5), cytosine (0.5), guanine (0.5), thymine (2), and uracil (0.5). Additional components were $MgSO_4 \cdot 7H_2O$ (5), $FeCl_3$ (8), thiamine (1), niacin (1.2), biotin (0.005), calcium pantothenate (0.25), $ZnCl_2$ (0.07), $MnCl_2 \cdot 4H_2O$ (0.099), boric acid (0.006), $CoCl_2 \cdot 6H_2O$ (0.397), $CuCl_2 \cdot 2H_2O$ (0.003), $NiCl_2 \cdot 6H_2O$ (0.024), $Na_2MoO_4 \cdot 2H_2O$ (0.036), and glucose (5). The overnight culture was back-diluted to OD_{600} = 0.05 into fresh minimal media at pH 7.4, pH 5.5, or pH 7.4+5 mM H_2O_2. Back-diluted cultures were shaken at 37^{o}C, 180 rpm for 1 to 2 hours before extraction of culture filtrate and cells for mass spectrometry.

Proteomics sample preparation

Protein was precipitated from 100 µL of each sample (either filtered media or bacterial cell lysate) by the addition of 900 µL of methanol, followed by centrifugation at 21,130 x g for 10 minutes. The supernatant of this precipitation was removed from the tube, leaving only the precipitated protein pellet, which was then resuspended for 5 min at 95 ^{o}C with shaking (1,000 rpm) in a 50 µL of 1% sodium deoxycholate in a 100 mM Tris-HCl buffer at pH 8.0. Following protein concentration determination by a Bradford assay, 30 µg of protein from each sample was then transferred to a new tube and reduction and alkylation of cysteine disulfide bonds was performed by the addition of 10 mM TCEP (tris(2-carboxyethyl)phosphine) and 40 mM 2-choloracetamide for 5 min at 45 ^{o}C with shaking (1,500 rpm). Digestion of proteins into peptides was initiated by the addition of 1 µg of LysC (Wako) and 0.5 µg of trypsin (Promega), followed by overnight incubation at 37 ^{o}C. Digestion was quenched by the addition of 10% trifluoroacetic acid until a pH of ~2-3 was reached. The digested lysates were clarified by centrifugation for 3 min at 21,130 x g, and the clarified peptide lysate was desalted on C18 stage tips (Nest Group). The resulting

desalted peptides were dried by vacuum centrifugation, resuspended in 0.1% formic acid prior to MS analysis.

Mass spectrometry data acquisition and analysis

Approximately 0.6 µg of sample was injected into an Orbitrap Fusion Lumos Tribrid Mass Spectrometer (Thermo Scientific) operated in positive ion mode using an EASY-nLC 1200 UHPLC (Thermo Scientific). Peptides were separated over a 75-µm internal diameter × 25-cm long picotip column packed with 1.9 µM C18 particles (Dr. Maisch) at a flow rate of 300 nL/min. Buffer A was comprised of 0.1% formic acid, and buffer B was comprised of 80% acetonitrile in 0.1% formic acid. Peptides were eluted by a linear gradient of 1 to 28% B over 25 minutes, followed by a 7 min ramp from 28 to 32% B, and finally a 3 min ramp to 95% buffer B and a subsequent 10min wash at 95% buffer B. MS data was collected over a 45 minutes total acquisition time with MS1 detection in the Orbitrap at 240K resolution in profile mode, 250-1350 m/z scan range, a 50 ms maximum injection time, a $1x10^6$ AGC target, a 30% RF lens setting, a 275 ^oC transfer tube temperature, and a 2 kV spray voltage. Data dependent MS2 scans were performed in centroid mode using Advanced Peak Determination on charge states from 2-6, with a +/- 10 ppm exclusion for a duration of 40 seconds after one observation. Selected precursors were isolated with a 0.7 m/z window and fragmented with a 32% normalized HCD energy in the ion trap with a rapid scan rate, a 200-1200 m/z range, a 20ms maximum injection time, a $3x10^5$ AGC target.

Raw data was searched against the *Staphylococcus aureus* (strain USA300) Uniprot protein database (downloaded July 5, 2020) using Maxquant (version 1.6.12.0) (67). Default search parameters were used, including a minimum peptide length of 7 amino acids, variable modification of acetylation of the protein N-terminus, variable modification of oxidation on methionine, match between runs was disabled, and peptides and protein were filtered to a 1% false discovery rate. MS1 area under the curve intensity values were then analyzed by SAINTexpress (68) was used to confidently discriminate secreted bacterial proteins from contaminating cellular proteins. Proteins with a SAINTexpress BFDR < 0.05 were considered to be high-confidence *Staphylococcus aureus* secreted proteins.

Bone-marrow macrophage infection assay

Overnight MRSA cultures were prepared by inoculating LB broth with WT or transposon-inserted mutant MRSA USA300 JE2 strain and culturing overnight at 37^{o}C, 180 rpm. ~16 hours later, overnight cultures were back-diluted in fresh LB broth at OD_{600} = 0.05 and cultured for ~2 hours to mid-log growth (OD_{600} = ~0.5). At mid-log growth phase, MRSA cultures were washed twice 1x PBS, pH 7.4. Final resuspension of MRSA pellet was with Bone-marrow-derived macrophage (BMDM) media.

For CFU measurements, BMDMs were spin-fected with MRSA in BMDM media at 1,200 rpm for 5 minutes for a MOI = 10. After spin-fection, BMDMs were washed once with 1x PBS, pH 7.4, then incubated at 37 ºC, 5% CO_2 for 20 hours in BMDM media containing 100 µg/mL gentamicin (Sigma-Aldrich G1397). BMDMs were lysed while suspended in Milli-Q water for 10 minutes at room temperature. Intracellular MRSA was plated on LB agar plates and incubated overnight at 37 ºC.
For LDH measurements, BMDMs were suspended in BMDM media containing MRSA at a MOI = 10. Uninfected BMBM wells and empty wells were suspended in BMDM media alone. Then, plates were incubated at 37 ºC, 5% CO_2 for 6 hours. 10x (10% v/v) Triton-X in Milli-Q water was added to positive control well. Media from BMDM plates was mixed 1:1 LDH working reagent (20 µL of 36 mg/mL Lithium L-lactate (Sigma Aldrich L2250) in 10 mM Tris buffer, pH 8.5; 2 µL of 20 mg/mL Iodonitrotetrazolium chloride (Sigma Aldrich I8377) in DMSO; 2 µL of 13.5 U/mL Diaphorase (Roche 10411558001), 3 mg/mL NAD+ (Sigma Aldrich N3014), 0.03% w/v BSA, 1.2% w/v sucrose in 1x PBS, pH 7.4; and 36 µL of 1% w/v BSA in 1x PBS, pH 7.4; per reaction) and incubated at room temperature for 30 minutes covered from light. LDH release assay reaction products were mixed 1:1 with 10% formalin and measured absorbance at 490 nm.

RNA extraction, reverse transcription, and PCR

WT MRSA USA300 JE2 culture in LB media was grown overnight at 37 ºC, 180 rpm. The next morning, the overnight culture was backdiluted into LB media to OD_{600} = 0.05 then shaken at 37 ºC, 180 rpm for 2 hours and 30 minutes. MRSA cells were pelleted and lysed with TRIzol reagent (Invitrogen 15596026), bead beaten with 0.1 mm silica beads (MP 116911100) using Mp FastPrep-24 Bead Beater (MP 116004500). Bead beaten TRIzol cell extracts were given chloroform and phase separated with centrifugation at 12,000 rcf, 10 minutes, 4 ºC. RNA was extracted and purified using the RNeasy mini kit (Qiagen 74104) with on-column DNase digest. Reverse transcription was performed with Superscript III Reverse Transcriptase kit (Invitrogen 18080093) and reverse transcription primers specific for either SAUSA300_1739, SAUSA300_1740, or SAUSA300_1744 (Table 1). Reverse transcription product was used for PCR reaction with Q5 DNA polymerase kit (NEB M0491L) with forward primer specific for SAUSA300_1739 and reverse primers specific for either SAUSA300_1739, SAUSA300_1740, or SAUSA300_1744. PCR products were run on 1% w/v agarose gel in TAE buffer.

Genetic analysis of SAUSA300_1739 to SAUSA300_1744 operon

Phylogenetic tress of *S. aureus* strains were constructed using the tool VBCG (69) with default parameters. *S. aureus* operon *SAUSA300_1739-SAUSA300_1744* nucleotide coding sequences from USA300 FPR3757 strain were used to query an NCBI BLAST database of *S. aureus* reference genomes to identify the operon in other strains. Heatmaps depicting percent identity were generated in Prism.

Accessed online through the National Center for Biotechnology Information (NCBI) repository whole genome sequences of *Staphylococcus aureus* strains: COL (NCBI accession number: CP000046), JP080 (NCBI accession number: AP017922.1), KAM440 (NCBI accession number: AP040133.1), Newman (NCBI accession number: AP009351.1), MRSA252 (NCBI accession number: BX571856.1), JKD6008 (NCBI accession number: CP002120.1), MSSA476 (NCBI accession number: NC_002953.3), NCTC 8325 (NCBI accession number: NC_007795.1), 04-02981 (NCBI accession number: NC_017340.1), 6850 (NCBI accession number: NC_022222.1), ED133 (NCBI accession number: NC_017337.1), JKD6159 (NCBI accession number: NC_017338.2), Mu3 (NCBI accession number: AP009324.1), RF122 (NCBI accession number: NC_007622.1), TCH60 (NCBI accession number: CP002110.1), VC40 (NCBI accession number: NC_016912.1), N315 (NCBI accession number: NC_002745.2), USA300_FPR3757 (NCBI accession number: CP000255.1), 08BA02176 (NCBI accession number: NC_018608.1), 71193 (NCBI accession number: NC_017673.1), ED98 (NCBI accession number: NC_013450.1), JH9 (NCBI accession number: NC_009487.1), LGA251 (NCBI accession number: FR821779.1), Mu50 (NCBI accession number: NC_002758.2), ST398 (NCBI accession number: NC_017333.1), TW20 (NCBI accession number: FN433596.1), JSNZ (NCBI accession number: CM129921.1), 11819-97 (NCBI accession number: NC_017351.1), EXT-R 2 (NCBI accession number: NC_017343.1), HO 5096 0412 (NCBI accession number: NC_017763.1), M013 (NCBI accession number: NC_016928.2), MW2 (NCBI accession number: NC_003923.1), T0131 (NCBI accession number: NC_017347.1), USA300_TCH1516 (NCBI accession number: NC_010079.1), LAC (NCBI accession number: NZ_CP055225.1), C8879 (NCBI accession number: NZ_CP020956.1), JK3137 (NCBI accession number: NZ_CP020960.1), USA400-0051 (NCBI accession number: CP019574.1), 2395 (NCBI accession number: NZ_CP007499.1), CA-347 (NCBI accession number: NC_021554.1), CMRSA-3 (NCBI accession number: NZ_CP029685.1), UCI 28 isolate ST5 (NCBI accession number: NZ_CP018768.1), UCI62 (NCBI accession number: NZ_CP018766.1), ISU935 isolate ST5 (NCBI accession number: NZ_CP017090.1), SA40 (NCBI accession number: NC_022443.1), USA300_SUR1 (NCBI accession number: CP009423.1), 3488_VV_ST8 (NCBI accession number: NZ_CP089502.1), Gv69 (NCBI accession number: CP009681.1), BSN170 (NCBI accession number: NZ_CP151257.1), BSN08 (NCBI accession number: NZ_CP186027.1), Alexandria_2020-19 (NCBI accession number: CP113244.1), RIVM_M083782 (NCBI accession number: NZ_CP096532.1), 8253 (NCBI accession number: CP166864.1), 9888 (NCBI accession number: CP166863.1), and ST772-MRSA-V strain DAR4145 (NCBI accession number: CP010526.1).

Generation of genomic knockouts and complementation

WT MRSA USA300 JE2 genomic DNA was purified using NEB Monarch Genomic DNA Purification Kit (NEB T3010S) and Lysostaphin (Millipore Sigma SRE0053). 1 kb upstream and downstream of coding regions of *SAUSA300_1739* and *SAUSA300_1740* were cloned from MRSA genomic DNA and cloned into pIMAY using NEBridge Golden Gate Assembly Kit (BsaI-HF v2) (NEB E1602) with pIMAY-GG-fwd and pIMAY-GG-rev primers listed in table 2. *SAUSA300_1741* to *SAUSA300_1744* coding regions were cloned from MRSA genomic DNA and cloned into pIMAY using NEB Gibson Assembly Cloning kit (NEB E5510S) and pIMAY-GA-fwd and pIMAY-GA-rev primers listed in table 2. pIMAY constructs containing 1 kb upstream and 1 kb downstream of each gene were first transformed into DH5α, then plasmids from DH5α were transformed into IM08B (70). Plasmids purified from IM08B were electroporated in WT MRSA USA300 JE2 strain. Genetic manipulation of WT MRSA USA300 JE2 strain was performed as described in Monk, et al., 2012, to generate knockouts of *SAUSA300_1739* to *SAUSA300_1744*.
Complements were generated by cloning coding regions of each gene *SAUSA300_1739* to *SAUSA300_1744* from purified WT MRSA USA300 JE2 genomic DNA using primers GI-fwd and GI-rev primers, and amplification of pRN11 backbone removing the mCherry gene (71) with primers backbone-fwd and backbone-rev primers listed in Table 3. PCR products were annealed together with NEB Gibson Assembly Cloning kit (NEB E5510S). Plasmids were transformed into DH5α, then plasmids from DH5α were transformed into IM08B (70). Plasmids purified from IM08B were electroporated into genomic knockouts of gene encoded in modified pRN11 expression plasmids (i.e. Δ*SAUSA300_1739* JE2 was electroporated with pRN11-1739).

Murine subcutaneous infection model

The day prior to infection, WT C57BL/6 (Inotiv C57BL/6JRccHsd) mice had lower back region between back and right hind leg shaved. On the day of infection, overnight MRSA cultures in LB media were back-diluted to OD_{600} = 0.05 in fresh LB media and cultured at 37ºC, 180 rpm for 2 hours 15 minutes. Once MRSA culture has reached mid-log growth phase (OD_{600} = ~0.5), MRSA cells were washed twice with 1x PBS, pH 7.4. MRSA cells were final resuspension in 1x PBS, pH 7.4 and diluted down to 1 x 10^8 CFU/mL. Anesthetized mice were subcutaneously injected with 1 x 10^7 CFU in shaved region of lower right back of mice between spine and right back leg. 3 days post-infection, mice were euthanized. Lesion sizes were measured with caliper and extracted with 12 mm biopsy punch (Acuderm P1225). Following bead beating and serial dilutions, homogenized lesion samples were plated on LB agar plates which were incubated overnight at 37 ºC.

Expression of SAUSA300_1739 and SAUSA300_1740 in *E. coli* BL21 cells

WT MRSA USA300 JE2 genomic DNA was PCR'ed to clone *SAUSA300_1739* and *SAUSA300_1740* open-reading frames with removal of the N-terminal sec-Lipo sequence

and addition of 6x His-tag on C-terminus. Open-reading frames were cloned into *E. coli* expression plasmid pET14b. pET14b encoding *SAUSA300_1739* or *SAUSA300_1740* were transformed into BL21 cells (NEB C2527H). BL21 colonies with either pET14b-*SAUSA300_1739* or pET14b-*SAUSA300_1740* were inoculated in LB broth with antibiotic selection and grown at 37 ^{o}C, 180 rpm. Once cultures reached mid-log growth, IPTG was added at 1 mM final concentration and cultures were shaken at 16 ^{o}C, 180 rpm overnight.

After overnight induction, BL21 cells were lysed with CelLytic B cell Lysis Reagent (Sigma-Aldrich B7435). Cell lysate was incubated with 5 mL Ni-NTA resin (GoldBio H-350-50) in 20 mL gravity column. Ni-NTA beads were washed twice with 20 mL first wash buffer (25 mM Tris-HCl, 150 mM NaCl, 20 mM Imidazole, pH 7.6), then washed once with 20 mL second wash buffer (25 mM Tris-HCl, 150 mM NaCl, 40 mM Imidazole, pH 7.6), and eluted with 10 mL elution buffer (25 mM Tris-HCl, 150 mM NaCl, 350 mM Imidazole, pH 7.6). Protein was concentrated and buffer exchanged into final suspension buffer (100 mM NaCl, 25 mM Tris-HCl, 10% v/v glycerol, pH 7.6) using centrifugal concentrator (Millipore UFC9003).

DNase activity assay

Modified pRN11 plasmid, pAZ14, was linearized using EcoRI digestion (NEB R3101L) to make a 6 kb linear DNA product. 100 ng of linearized pAZ14 was incubated in reaction buffer (3 mM $MgCl_2$, 50 mM NaCl, 10 mM Tris-HCl, pH 8.0) with purified SAUSA300_1739 or SAUSA300_1740 at designated concentrations (1,000 nM, 2,000 nM, or 5,000 nM) with or without EDTA (25 mM) and incubated at 37 ^{o}C for designated timepoints (0.5 hours, 1 hour, 2 hours, 4 hours, or 8 hours). DNase reaction products ran on 1% w/v agarose gels at 100 V for 40 minutes.

Data availability

All raw MS data files, search results and individual spectral libraries are available from the Pride partner ProteomeXchange repository (72).

Results

Characterization of MRSA USA300 secreted proteome

We first developed an exoproteome of MRSA USA300 to identify surface and secreted proteins in an unbiased manner. To establish the exoproteome, an overnight culture of WT MRSA USA300 SF8300 strain in minimal media at pH 7.4 was back-diluted to OD_{600} = 0.05 in fresh minimal media at pH 7.4, pH 5.5, or pH 7.4 + 5 mM H_2O_2. We chose pH 5.5 as the acidic condition because MRSA USA300 has been shown to prevent phagolysosome maturation with a final pH of ~5 within the phagosomes of THP-1 macrophages infected with MRSA USA300 (73). Likewise, the 5 mM H_2O_2 concentration was chosen as the oxidative stress condition to mimic an oxidative environment of a phagosome. After 1 and 2 hours shaking at 37^{o}C, the supernatants and pellets were processed and characterized via electrospray ionization mass spectrometry. A total of 109 proteins were found to be significantly more abundant in the collected supernatant than the pellet (Supplementary Table 1). Of the 109 proteins, 52 proteins have Sec/SPI signal peptides, 23 proteins have Sec/SPII signal peptides designated for lipoproteins, 6 proteins have been published as secreted proteins, and 9 proteins are transmembrane proteins. 70 proteins have been previously published to have a role as *S. aureus* virulence factors; however, 29 proteins have not been characterized and unknown if they contribute to *S. aureus* virulence.

SAUSA300_1739 and *SAUSA300_1740* have differences in virulence compared to WT MRSA in-vitro

Of the 109 proteins collected in this exoproteome, 23 are uncharacterized. Corresponding transposon mutants in the genes of 21 of these proteins were selected from the Nebraska Transposon Mutant Library (NTML) which contains individual arrayed transposon-inserted mutants of all non-essential genes of the *Staphylococcus aureus* genome (74). We first assayed each transposon mutant for the ability to survive during macrophage infection, and for the ability to kill host macrophages. For bacterial CFU determination C57BL/6 (B6) bone-marrow derived macrophages (BMDMs) were infected at MOI of 10 after which gentamicin was added to the media to eliminate extracellular bacteria. For cell killing assays, BMDM were infected and cultured without gentamicin and a lactate dehydrogenase (LDH) release assay was used to quantify cell death. The majority of mutants had no phenotype in either assay (not shown). Six mutants with transposon insertions in the genes *SAUSA300_1739, SAUSA300_1740, SAUSA300_0883, SAUSA300_2355, SAUSA300_0651,* and *SAUSA300_2315* exhibited differences in CFU and or LDH release assay relative to the WT strains (Figure S1 and 1A, 1B), however these differences were modest.

MRSA encodes at least 3 secreted nucleases, Nuc1, Nuc2 (65), and EssD (66) (also called EsaD) that are important for virulence. Nuc1 is secreted, while Nuc2 remains cell associated (65). EssD is secreted through the type VIIb secretion system of *S. aureus*

(66). Interestingly, two of the secreted proteins identified in our exoproteome, SAUSA300_1739 and SAUSA300_1740 are annotated as potential DNA binding proteins/potential nucleases (Supplementary Figure X). These genes are contained within the same predicted operon. We observed statistically significant, but very minor differences in survival in macrophages comparing WT (JE2) with *SAUSA300_1739*::tn and *SAUSA300_1740*::tn mutants (Figure 1A, 1B). Similarly, minimal differences in macrophage cell death were elicited by these mutants relative to WT (Figure 1C, 1D).

_SAUSA300_1739_ and _SAUSA300_1740_ belong to an operon of 6 genes with no impact on axenic culture growth rates

Because genes located within an operon are transcriptionally controlled by the same promoter, a reasonable prediction about genes within an operon is that they might be involved in the same cellular processes (75). Since *SAUSA300_1739* and *SAUSA300_1740* are located next to each other in the MRSA USA300 FPR3757 genome, we tested whether *SAUSA300_1739* and *SAUSA300_1740* are transcribed in the same operon. The online Prokaryote Promoter Prediction v2.0 software predicted that there is only 1 promoter sequence between *SAUSA300_1738* and *SAUSA300_1745*, located upstream of *SAUSA300_1739*, suggesting that the genes between *SAUSA300_1739* to *SAUSA300_1744* may be transcribed together (76) (Figure 2A). To test this, we used reverse transcriptase-PCR (77) of purified WT MRSA USA300 JE2 mRNA using primer sets spanning putative gene junctions across the operon (Figure 2A) and found that that *SAUSA300_1739* to *SAUSA300_1744* are encoded on the same mRNA (Figure 2B). Thus, *SAUSA300_1739* and *SAUSA300_1740* belong to an operon of six genes from *SAUSA300_1739* to *SAUSA300_1744*.

_SAUSA300_1739_ to _SAUSA300_1744_ knockouts are attenuated in a mouse subcutaneous infection model

We next generated mutants lacking each individual gene of *SAUSA300_1739* to *SAUSA300_1744* in JE2 using allelic replacement with the pIMAY plasmid (78). We also generated complemented strains by transforming each individual mutant with modified expression plasmid pRN11 (71) that had the mCherry reading frame replaced with each of the individual genes PCR amplified from WT MRSA USA300 JE2 chromosomal DNA. All six mutants grew normally in LB broth at pH 7.4, pH 5.5, and pH 7.4+5 mM H_2O_2 conditions (Figure 2C, 2D, 2E). These results indicate that loss of any of the 6 genes in the *SAUSA300_1739* to *SAUSA300_1744* operon does not impact growth rate in broth at physiologically relevant pH, acidic, or oxidative stress conditions. To investigate if each of these 6 genes has a role in *S. aureus* pathogenesis, we infected WT B6 mice with WT, mutant, or complemented strains using a mouse subcutaneous infection model. WT C57BL/6 mice had right lower flanks shaved and were injected with 1 x 10^7 CFU MRSA. The infection was allowed to proceed for 3 days, at which time lesions were excised using

a 12 mm biopsy punch, homogenized, and CFU were enumerated by plating on agar. Surprisingly, each of the mutants had lower lesion CFU of >1 log compared to WT JE2, 3 days post-infection (Figure 4A, 4B). Each mutant was fully complemented by expression of the corresponding gene (Figure 4A, 4B). Additionally, each of the knockouts caused infections with reduced lesion size area compared to WT ns complemented strains at 3 days post-infection (Figure 4B). Taken together, these results indicate that each of the 6 genes in the *SAUSA300_1739* to *SAUSA300_1744* operon is important for *S. aureus* pathogenicity.

Genetic analysis of *SAUSA300_1739* to *SAUSA300_1744* across several *Staphylococcus aureus* strains

The pangenome of *Staphylococcus aureus* is highly diverse with only ~75% of the genome being conserved between *S. aureus* strains (79). The remaining ~25% of the *S. aureus* genome consists of mobile genetic elements including pathogenicity islands and plasmids that encode virulence factors (79). Since the ideal candidate for virulence factor-specific therapeutics and vaccine antigens should be highly conserved amongst *S. aureus* strains (80, 81), we examined the conservation of the *SAUSA300_1739* to *SAUSA300_1744* operon among 55 *S. aureus* strains including several community-acquired and hospital-acquired MRSA strains. The *SAUSA300_1739* to *SAUSA300_1744* operon is highly conserved (%nucleotide identity >90%) across the strains. (Figure 3). Interestingly, *SAUSA300_1741* and *SAUSA300_1742*—predicted to encode a lipoprotein and a cytoplasmic protein, respectively—split into two separate genes within the USA300 clonal lineage. Most USA300 (ST8, CC8) strains examined (SUR1, FPR3757, LAC, TCH1516, and JK3137) carry *SAUSA300_1741* and *SAUSA300_1742* as distinct genes, whereas the closely related USA300 strain C8897 (82) retains the ancestral single-gene configuration. This architecture matches what is found in the majority of *S. aureus* strains tested. These results indicate that the *SAUSA300_1739* to *SAUSA300_1744* operon is generally conserved across *S. aureus* strains, consistent with an important role in virulence.

SAUSA300_1739 and SAUSA300_1740 has DNase activity

SAUSA300_1739 and *SAUSA300_1740* are homologous to DNase and DNA-binding proteins (Supplementary Table 2). To test if SAUSA300_1739 and SAUSA300_1740 has DNase activity, we purified both proteins expressed in BL21 E. coli under IPTG induction along with Ni-NTA resin to purify 6xHIS-tagged proteins. Purified mature unacylated SAUSA300_1739 or SAUSA300_1740 were incubated at 1,000 nM, 2,000 nM, or 5,000 nM of purified with 100 ng of linearized DNA with or without 25 mM EDTA in a Magnesium-containing reaction buffer for indicated times. SAUSA300_1739 had demonstrable DNase activity at 5000nM (Figure 5A) that was abolished in the presence of EDTA, a divalent cation chelator and inhibitor of DNase (83) (Figure 5B).

SAUSA300_1740 showed somewhat greater DNase activity with DNAse activity observed at 1000nM (Figure 5C). The addition of EDTA also inhibited DNase activity of SAUSA300_1740 (84) (Figure 5D). These results support the idea that that SAUSA300_1739 and SAUSA300_1740 are secreted nucleases that promote the virulence of MRSA.

Discussion

The opportunistic pathogen *Staphylococcus aureus* remains a global burden causing serious and deadly infections. Approximately 20% of humans are persistent carriers, while an additional 60% of humans are intermittently colonized with *S. aureus* reinforcing the importance of studying this major pathogen (85). The rise of antibiotic resistance, the decline of novel antibiotic therapeutic development, and the lack of a protective vaccine all contribute to *S. aureus* remaining a leading cause of human infection. In addition, *S. aureus* is known to utilize an arsenal of virulence factors to evade and manipulate the immune system, lyse host cells, breakdown host antimicrobial molecules, among other mechanisms (64). A greater understanding of how important virulence factors promote *S. aureus* pathogenicity is necessary for anti-virulence factor therapeutic and vaccine development.

To find new virulence factors used by *S. aureus* to promote infection we first focused on identifying uncharacterized proteins secreted by the bacteria. Using this approach, we identified SAUSA300_1739 and SAUSA300_1740 as unknown-function lipoproteins secreted by MRSA JE2. We discovered that *SAUSA300_1739* and *SAUSA300_1740* are members of an operon of 6 genes, *SAUSA300_1739* to *SAUSA300_1744*. The loss of any of these 6 genes does not impact growth of MRSA in axenic culture including in acidic or oxidative conditions (86). Similarly, these genes do not play a large role in the ability of MRSA to survive inside of or kill host cells. Interestingly, *SAUSA300_1739* and *SAUSA300_1740* transposon-inserted MRSA USA300 mutants were hits identified in a screen for mutants that induce less cell damage in an in vitro human endothelial cell line infection model (87), suggesting that these 2 genes have some role as virulence factors. However, there was no additional follow-up on these specific hits in the published study. We observed only minor differences in assays for macrophage killing, suggesting that regulation of cell death may not be a major function of these virulence factors. Additionally, we show for the first time that mutants lacking *SAUSA300_1739* and *SAUSA300_1740* are attenuated for virulence in vivo. Taken together, the data collectively suggests that these virulence factors likely impact responses that occur in vivo, and have less of an impact in cell based infections in vitro, a finding that is consistent with the hypothesis that these proteins function as nucleases.

In addition to *SAUSA300_1739* and *SAUSA300_1740*, we found that every gene in the operon is required for full virulence of MRSA in skin infections. Previously, a transposon-insertion mutant of *SAUSA300_1741* MRSA USA300 was reported to be attenuated in a murine subcutaneous infection model while not impacting in-vitro growth (88). However, to our knowledge, nothing is known about the other genes in the operon, and their possible roles in virulence. Importantly, we found that the *SAUSA300_1739* to *SAUSA300_1744* operon is generally conserved in *S. aureus* strains. *SAUSA300_1740* in particular is highly conserved across majority of analyzed *S. aureus* strains. *SAUSA300_1740*, a now confirmed expressed lipoprotein virulence factor, could be an

ideal candidate for anti-virulence factor therapeutics and antigen for antibody-mediated vaccine due to its presence of the outside of the bacterial cell surface, inhibition of virulence factor mechanism, and conservation in the *S. aureus* genome (79, 80). Future works focused on antibody or small molecule drug-mediated inhibition of SAUSA300_1740 as well the antigenicity of SAUSA300_1740 could improve *S. aureus* infection treatment and vaccine development.

Previously there was almost nothing known about the functions of *SAUSA300_1739* and *SAUSA300_1740.* Protein blast searches suggested both proteins have DNase or DNA-binding activity. Our data indicates that *SAUSA300_1739* and *SAUSA300_1740* both encode DNases. *S. aureus* is known to utilize surface and secreted nucleases to regulate biofilm formation for immunoevasion, to breakdown antimicrobial neutrophil extracellular traps (NETs), and to produce cytotoxic concentrations of deoxyribonucleotides (65, 89). In the future, it will be important to identify the redundancies and differences in biochemical mechanisms of *Staphylococcus aureus* secreted nucleases nuc1, nuc2 (65), EssD (66), and newly identified SASUA300_1739, and SAUSA300_1740. In summary, we have identified that the *SAUSA300_1739* to *SAUSA300_1744* operon encodes 6 novel virulence factors with *SAUSA300_1739* and *SAUSA300_1740* having DNase activity and the remaining 4 genes with unknown function. From this work, our understanding of the *S. aureus* virulence factors important for establishing skin and soft tissue infections expands. Moving forward, it will be important to discover the functions of the 4 remaining genes of this operon and figure out the relationship between all 6 genes.

Acknowledgements
We acknowledge funding from the National Institutes of Health grant U19AI135990 to N.J.K. We thank Binh Diep's lab for the kind gift of WT MRSA USA300 SF8300 strain. The WT MRSA USA300 JE2 strain was provided by the Network on Antimicrobial Resistance in *Staphylococcus aureus* (NARSA) for distribution through BEI Resources, NIAID, NIH: *Staphylococcus aureus* subsp. *aureus*, Strain JE2, NR-46543. The Nebraska Transposon mutant library was provided by the Network on Antimicrobial Resistance in *Staphylococcus aureus* (NARSA) for distribution through BEI Resources, NIAID, NIH: Nebraska Transposon Mutant Library (NTML) Screening Array, NR-48501.

Figures

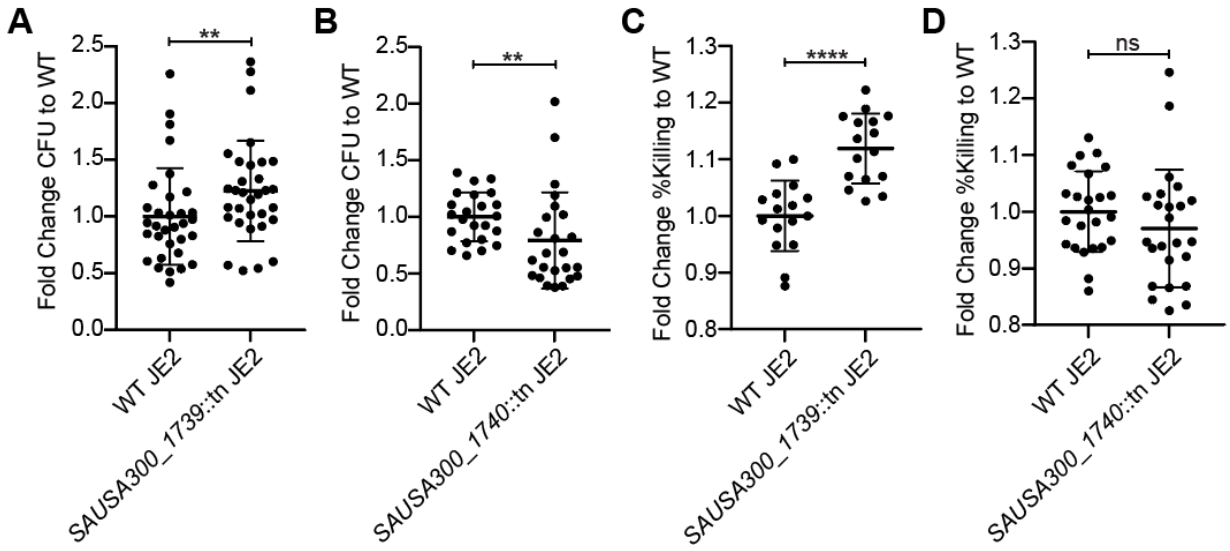

Figure 1. Transposon-inserts of *SAUSA300_1739* and *SAUSA300_1740* show differences in virulency compared to WT MRSA in-vitro. WT, *SAUSA300_1739*::tn, and *SAUSA300_1740*::tn MRSA USA300 JE2 were spinfected into WT C57BL/6 bone-marrow-derived macrophages (BMDMs) at a MOI of 10 followed by gentamicin protection for intracellular MRSA CFU, or BMDMs were infected without spinfection with MRSA at MOI of 10 for Lactate Dehydrogenase (LDH) release assay. **(A, C)** Intracellular CFU of MRSA after 20 hours post spinfection. Fold change CFU results in A and C are from comparison of individual biological replicates against the average WT MRSA USA300 JE2 CFU within the same experiment. **(B, D)** LDH release assay results of MRSA after 6 hours post-infection. Fold change %Killing LDH results in B are from comparison of individual biological replicates against the average WT MRSA USA300 JE2 %Killing LDH within the same experiment. **(A)** *SAUSA300_1739* results are from fold change CFU results of 5 pooled experiments and **(B)** *SAUSA300_1740* results are from fold change CFU results of 3 pooled experiments. **(C)** *SAUSA300_1739* results are from fold change LDH results of 2 pooled experiments and **(D)** *SAUSA300_1740* results are from fold change LDH results of 3 pooled experiments. **, $p < 0.01$; ****, $p < 0.0001$ (unpaired nonparametric Mann-Whitney U test).

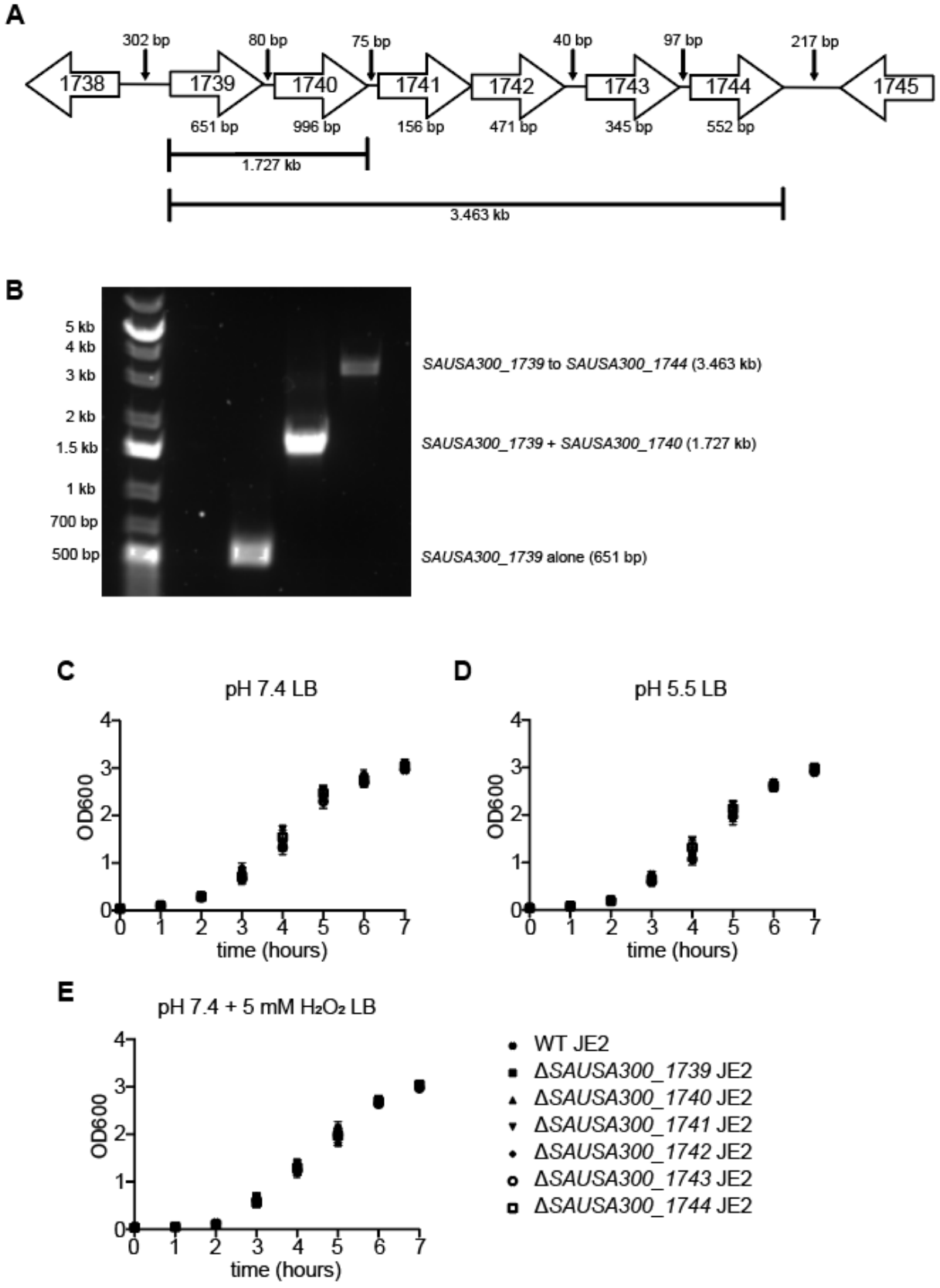
A
302 bp
80 bp
75 bp
40 bp
97 bp
217 bp
1738
1739
1740
1741
1742
1743
1744
1745
651 bp
996 bp
156 bp
471 bp
345 bp
552 bp
1.727 kb
3.463 kb
B
5 kb
4 kb
3 kb
2 kb
1.5 kb
1 kb
700 bp
500 bp
SAUSA300_1739 to SAUSA300_1744 (3.463 kb)
SAUSA300_1739 + SAUSA300_1740 (1.727 kb)
SAUSA300_1739 alone (651 bp)
C
pH 7.4 LB
OD600
time (hours)
D
pH 5.5 LB
OD600
time (hours)
E
pH 7.4 + 5 mM H2O2 LB
OD600
time (hours)
WT JE2
ΔSAUSA300_1739 JE2
ΔSAUSA300_1740 JE2
ΔSAUSA300_1741 JE2
ΔSAUSA300_1742 JE2
ΔSAUSA300_1743 JE2
ΔSAUSA300_1744 JE2

Figure 2. *SAUSA300_1739* and *SAUSA300_1740* are in an operon of 6 genes. WT MRSA USA300 JE2 was grown in LB broth overnight, then backdiluted to OD_{600} = 0.05 and shaken at 37 ºC, 180 rpm for 2.5 hours followed by whole RNA extraction and reverse-transcription PCR. **(A)** Representation of gene orientation and distances between *SAUSA300_1738* and *SAUSA300_1745*. **(B)** Agarose gel of reverse-transcription PCR after RNA extraction. Primers for reverse transcription were specific for *SAUSA300_1739*, *SAUSA300_1740*, or *SAUSA300_1744*. PCR of reverse transcription product was performed using forward primer specific for *SAUSA300_1739* and reverse primers specific for either *SAUSA300_1739*, *SAUSA300_1740*, or *SAUSA300_1744*. Results in B represent 3 biological replicates. WT, Δ*SAUSA300_1739*, Δ*SAUSA300_1740*, Δ*SAUSA300_1741*, Δ*SAUSA300_1742*, Δ*SAUSA300_1743*, and Δ*SAUSA300_1744* MRSA USA300 JE2 overnight cultures grown in LB pH 7.4 media was backdiluted into LB media at **(C)** pH 7.4, **(D)** pH 5.5, or **(E)** pH 7.4 with 5 mM H_2O_2. OD_{600} was measured every hour for 7 hours. Results in C, D, and E represent triplicate replicates for each timepoint and media conditions.

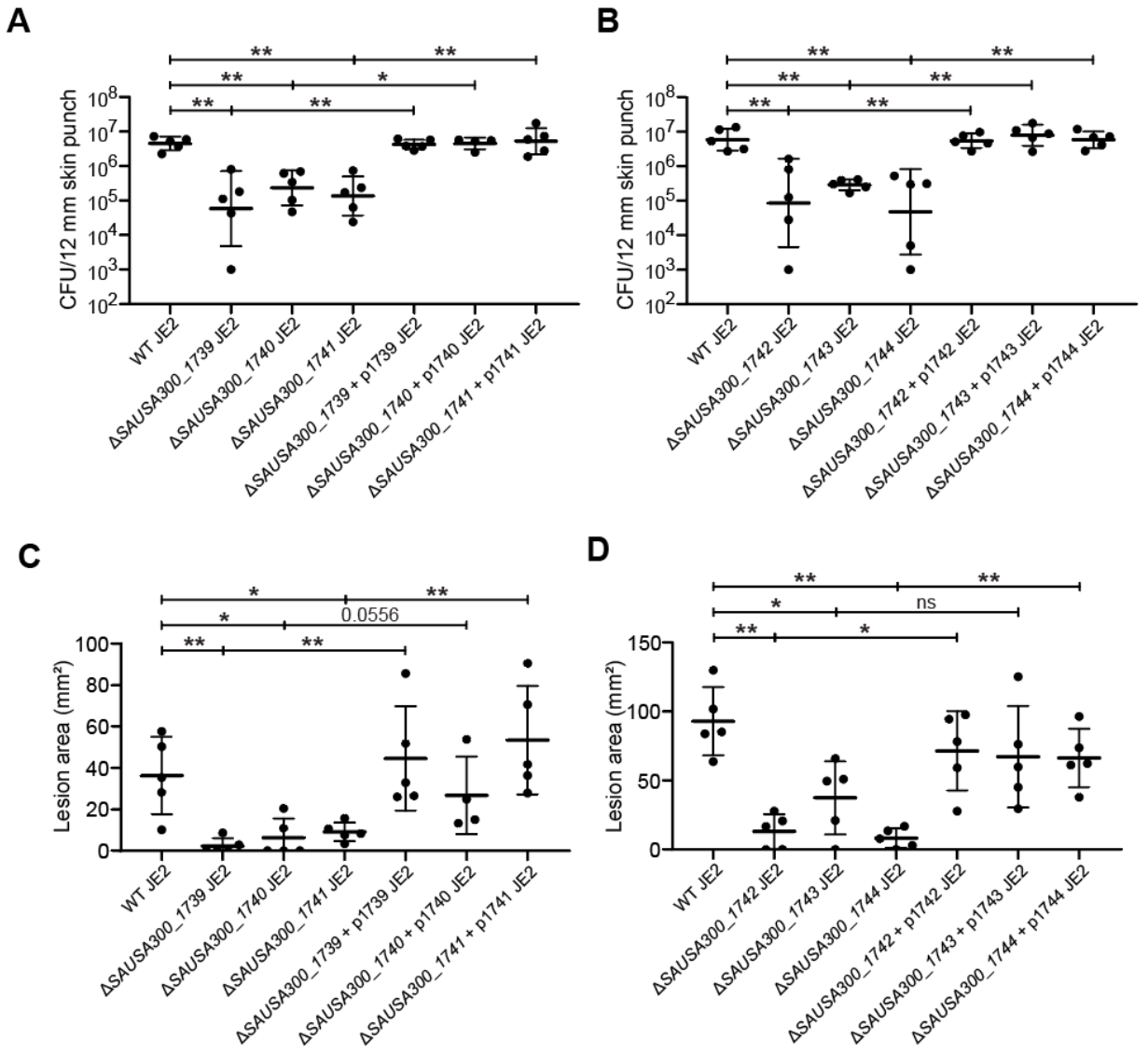

Figure 3. Genetic knockouts of either *SAUSA300_1739* to *SAUSA300_1744* results in attenuation in a murine subcutaneous infection model. WT C57BL/6 mice were infected with 1 x 10^7 CFU of either WT, Δ*SAUSA300_1739*, Δ*SAUSA300_1740*, Δ*SAUSA300_1741*, complemented Δ*SAUSA300_1739* (+ p1739), complemented Δ*SAUSA300_1740* (+ p1740), or complemented Δ*SAUSA300_1741* (+ p1741) MRSA USA300 JE2, or mice were infected with 1 x 10^7 CFU of either WT, Δ*SAUSA300_1742*, Δ*SAUSA300_1743*, Δ*SAUSA300_1744*, complemented Δ*SAUSA300_1742* (+ p1742), complemented Δ*SAUSA300_1743* (+ p1743), or complemented Δ*SAUSA300_1744* (+ p1744) MRSA USA300 JE2. **(A, B)** 3 days post-infection, CFU from standardized 12 mm skin biopsy punches. **(C, D)** 3 days post-infection, open lesion area using caliper. Results in A-D are representative of 2 independent experiments. *, $p < 0.05$; **, $p < 0.01$ (unpaired nonparametric Mann-Whitney U test).

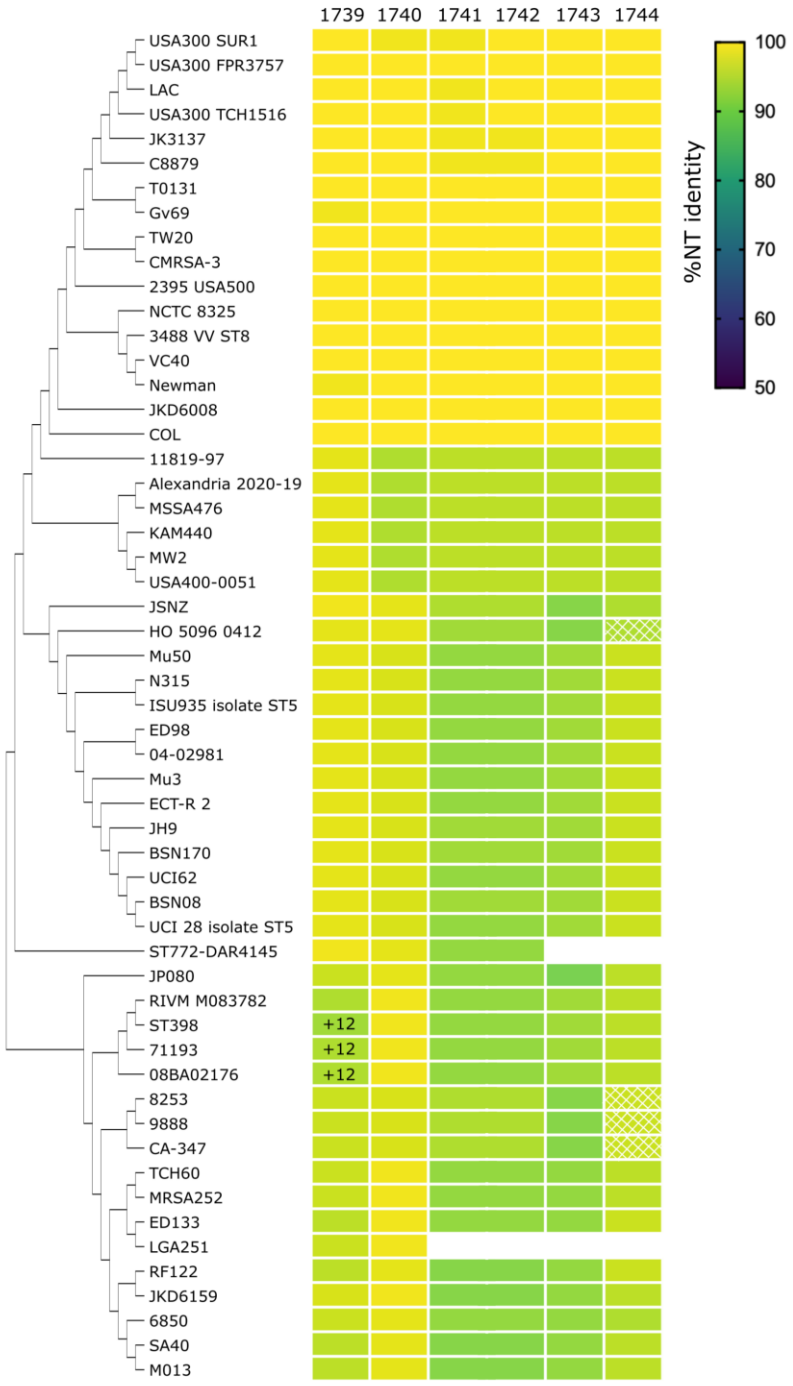

Figure 4. Genetic analysis of *SAUSA300_1739* to *SAUSA300_1744* operon. Whole genome sequences were obtained through the NIH National Center of Biotechnology Information (NCBI) repository, accession numbers listed in materials and methods section. Lack of box for gene indicates lack of gene in strain. “+12” indicates 12 base-pair in-frame insertion in gene of strain. Box with cross hatch marks indicates coding sequence is fully present but interrupted by some insert.

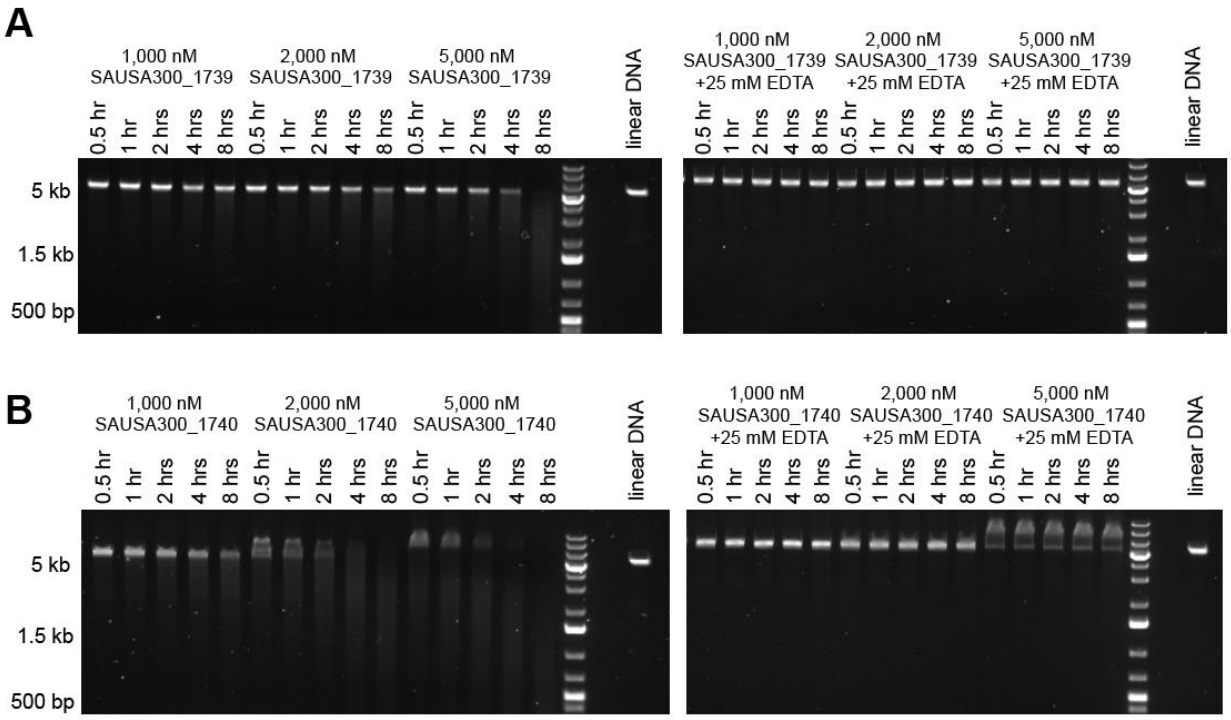

Figure 5. SAUSA300_1739 and SAUSA300_1740 have DNase activity. (A, B) 1,000, 2,000, or 5,000 nM purified mature unacylated SAUSA300_1739 was incubated with 100 ng of linear modified pRN11 plasmid (6 kb size) for 0.5, 1, 2, 4, or 8 hours at 37 ^{o}C in Magnesium-containing reaction buffer without EDTA **(A)** or with 25 mM EDTA **(B)**. **(C, D)** 1,000, 2,000, or 5,000 nM purified mature unacylated SAUSA300_1740 was incubated with 100 ng of linear modified pRN11 plasmid (6 kb size) for 0.5, 1, 2, 4, or 8 hours at 37 ^{o}C in Magnesium-containing reaction buffer without EDTA **(C)** or with 25 mM EDTA **(D)**. Each agarose gel image is representative of 3 independent experiments.

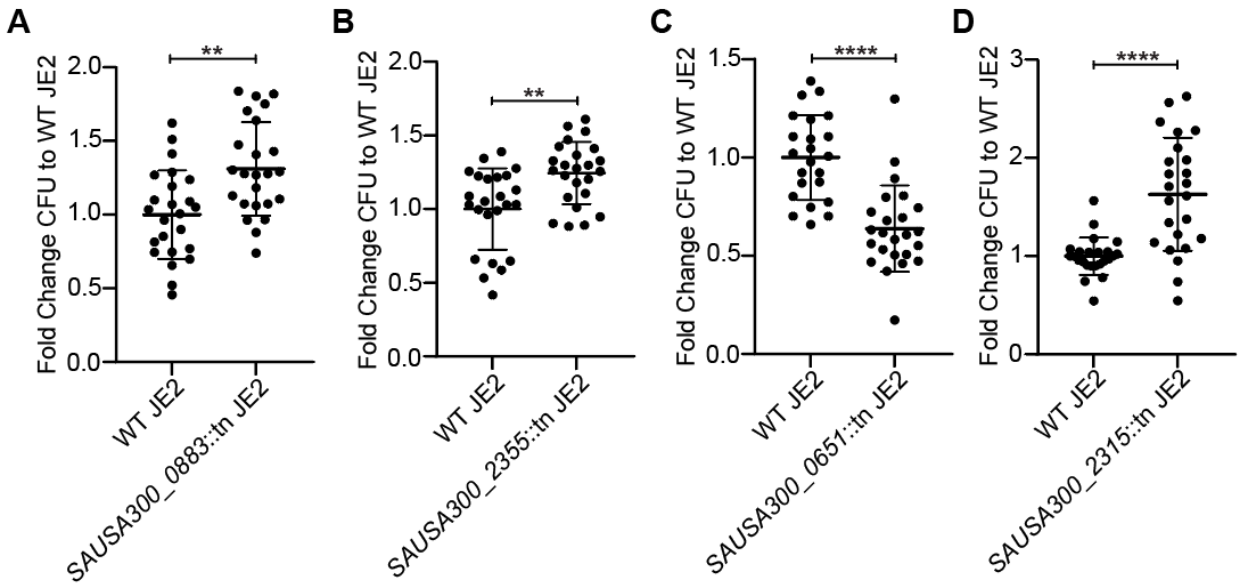

Supplementary Figure 1. Transposon insertion mutants with differences in virulence compared to WT MRSA. MRSA USA300 JE2 were spinfected into WT C57BL/6 bone-marrow-derived macrophages (BMDMs) at a MOI of 10 followed by gentamicin protection for intracellular MRSA CFU, or BMDMs were infected without spinfection with MRSA at MOI of 10 for Lactate Dehydrogenase (LDH) release assay. **(A)** Intracellular CFU of WT and *SAUSA300_0883*::tn MRSA USA300 JE2 after 20 hours post spinfection. **(B)** Intracellular CFU of WT and *SAUSA300_2355*::tn MRSA USA300 JE2 after 20 hours post spinfection. **(C)** Intracellular CFU of WT and *SAUSA300_0651*::tn MRSA USA300 JE2 after 20 hours post spinfection. **(D)** Intracellular CFU of WT and *SAUSA300_2315*::tn MRSA USA300 JE2 after 20 hours post spinfection. Fold change CFU results in A-D are from comparison of individual biological replicates against the average WT MRSA USA300 JE2 CFU within the same experiment. Each transposon-inserted mutant results for A-D are from fold change results of 3 pooled experiments. **, $p < 0.01$; ****, $p < 0.0001$ (unpaired nonparametric Mann-Whitney U test).

Table 1. Primer sequences for reverse transcription and PCR.

Primer name	Primer sequence (5’ -> 3’)
1739 RT primer	TTTATCAGGTTCACATGC
1740 RT primer	GGTTTGCTATGGGGCATGGGC
1744 RT primer	CTAATATTCCAGGCAAATAG
1739 forward PCR primer	CTGTTAAAAATTCTGAAAGACGCGGCATGTTAAAAGGA
1739 reverse PCR primer	TCTATCTAAATGTGGTCGATATGCTGGATGATCGG
1740 reverse PCR primer	GGTTTGCTATGGGGCATGGGC
1744 reverse PCR primer	CGCCAATGTACCAATCAATGACTGTTGGTTTG

Table 2. Primer sequences for making knockouts of *SAUSA300_1739* to *SAUSA300_1744*.

Primer name	Primer sequence (5’ -> 3’)
1739-1kb-up-fwd	ATCGGTGGTCTCCGCTGATAAGTATAAGATTCTTGACCGTCT
1739-1kb-up-rev	ATCGGTGGTCTCCTACATGATTTACTACATAAAACCTGGA
1739-1kb-down-fwd	ATCGGTGGTCTCCTGTAAACAACAAGCGAATTGAATTC
1739-1kb-down-rev	ATCGGTGGTCTCCATTGTATGGGGCATGGGC
1740-1kb-up-fwd	TGACCTGGTCTCGGCTGCTCTAAAAATAAATACAATATATTATAGCAAATAGAAA
1740-1kb-up-rev	TGACCTGGTCTCGTACATGCCTAAAAAATCTCCCTCA
1740-1kb-down-fwd	TGACCTGGTCTCGTGTAAAATTTCAGGGTAGCTCGG
1740-1kb-down-rev	TGACCTGGTCTCGATTGTAAACAGACTGTAACTGTGTCTT
pIMAY-GG-fwd	TACATGGTCTCACAATTCGCCCTATAGTGAGT
pIMAY-GG-rev	ACTAGGGTCTCACAGCTTTTGTTCCCTTTAGTG
1741-1kb-up-fwd	GGGAACAAAAGCTGGGTACCCAATGGGAACAATTCCAA
1741-1kb-up-rev	GTGTCATTTACATTTTTTTATCTCCTTGATTTGA
1741-1kb-down-fwd	TAAAAAAATGTAAATGACACCACAAGAAG
1741-1kb-down-rev	TATAGGGCGAATTGGAGCTCGCTACAGCTTGCGA
1742-1kb-up-fwd	GGGAACAAAAGCTGGGTACCGGCGACCTTGAAGT
1742-1kb-up-rev	TATGCCATTACATTTACTTTTCTGTATTTGACTG
1742-1kb-down-fwd	AAAGTAAATGTAATGGCATACTTTGATTAATCG
1742-1kb-down-rev	TATAGGGCGAATTGGAGCTCCCAGGCAAATAGGCA
1743-1kb-up-fwd	GGGAACAAAAGCTGGGTACCGTAGCTGTTGCGAGT
1743-1kb-up-rev	TATATGTCTACATAGCGTTTCTCCTAAAAAT
1743-1kb-down-fwd	AAACGCTATGTAGACATATAAAAGTCGAATGTAAC
1743-1kb-down-rev	TATAGGGCGAATTGGAGCTCCAGTTTTCAGTCGACTTACT
1744-1kb-up-fwd	GGGAACAAAAGCTGGGTACCCACTATTAACTGCCTGTG
1744-1kb-up-rev	GGAAATCTTACATTTCAATATACCTCTTTTCAAAC
1744-1kb-down-fwd	TATTGAAATGTAAGATTTCCTTGAGTCTAGAT
1744-1kb-down-rev	TATAGGGCGAATTGGAGCTCGGACAAAAATGAATATGAAGC
pIMAY-GA-fwd	GAGCTCCAATTCGCCCTATAGTGAGTCG
pIMAY-GA-rev	GGTACCCAGCTTTTGTTCCCTTTAGTGAG

Table 3. Primer sequences for cloning *SAUSA300_1739* to *SAUSA300_1744* coding regions and amplification of pRN11 backbone for complementation.

Primer name	Primer sequence (5’ -> 3’)
1739-GI-fwd	ATGTATACATATGAAAATAACATATAAATATAGAGGAGATTTACCT
1739-GI-rev	TTACGAATTCTTAATATTTATCAGGTTCACATGCAC
1740-GI-fwd	ATGTATACATATGAGCAATCAATTCAAAAGCG
1740-GI-rev	TTACGAATTCTTATTCTGTTGAAGCGTCGT
1741-GI-fwd	ATGTATACATATGAAATTCAAAGCTATCGTTGC
1741-GI-rev	TTACGAATTCTTACTTTTCTGTATTTGACTGTGTAGT
1742-GI-fwd	ATGTATACATATGACACCACAAGAAGCC
1742-GI-rev	TTACGAATTCTTATTTAACTTTAGTTTCTTCAGAATTATTTGC
1743-GI-fwd	ATGTATACATATGATAACATTTGAGAATATACAACAACTTG
1743-GI-rev	TTACGAATTCCTATTTCTCTTGTATAATACGCCAATTG
1744-GI-fwd	ATGTATACATATGGAGAAAAATGAATATATAGCTAAATATAATGAATATAG
1744-GI-rev	TTACGAATTCTTATATTTCTATTCCTTTTAACATATCGTCAATTT
1739-backbone-fwd	TAAATATTAAGAATTCGTAATCATGTCATAGCTG
1739-backbone-rev	TTATTTTCATATGTATACATCCTCCTAAGGTACC
1740-backbone-fwd	AACAGAATAAGAATTCGTAATCATGTCATAGCTG
1740-backbone-rev	GATTGCTCATATGTATACATCCTCCTAAGGTACC
1741-backbone-fwd	AGAAAAGTAAGAATTCGTAATCATGTCATAGCTG
1741-backbone-rev	TGAATTTCATATGTATACATCCTCCTAAGGTACC
1742-backbone-fwd	AGTTAAATAAGAATTCGTAATCATGTCATAGCTG
1742-backbone-rev	GTGGTGTCATATGTATACATCCTCCTAAGGTACC
1743-backbone-fwd	AGAGAAATAGGAATTCGTAATCATGTCATAGCTG
1743-backbone-rev	ATGTTATCATATGTATACATCCTCCTAAGGTACC
1744-backbone-fwd	AGAAATATAAGAATTCGTAATCATGTCATAGCTG
1744-backbone-rev	TTTTCTCCATATGTATACATCCTCCTAAGGTACC

Supplementary Table 1. Mass spectrometry results of proteins with higher abundance in culture filtrate than cell pellets.

uncharacterized protein (SAUSA300_0274)
lipoprotein (SAUSA300_0798)
Chitinase-related protein (SAUSA300_0964)
Uncharacterized protein (SAUSA300_0681)
Purine nucleoside phosphorylase DeoD-type (deoD)
Staphopain A (SAUSA300_1890)
Uncharacterized protein (SAUSA300_0754)
Uncharacterized protein (SAUSA300_2574)
Clumping factor A (clfA)
Uncharacterized protein (SAUSA300_0602)
Lipoprotein (SAUSA300_0437)
Staphlylococcal enterotoxin Q (seq)
Putative staphylocoagulase (SAUSA300_0773)
Excalibur domain-containing protein (SAUSA300_1739)
Fibrinogen-binding protein (SAUSA300_1052)
Lysostaphin (lytM)
Cell division protein FtsL (ftsL)
Triacylglycerol lipase (lip)
Micrococcal nuclease (nuc)
Secretory antigen SsaA (ssaA)
DUF2294 domain-containing protein (SAUSA300_0427)
Glycerophosphoryl diester phosphodiesterase (glpQ)
Molybdenum ABC transporter, molybdenum-binding protein ModA (modA)
Panton-Valentine Leukocidin (LukF-PV)
Putative lipoprotein (SAUSA300_0693)
PhiSLT ORF144-like protein, putative lipoprotein (SAUSA300_1436)
Cysteine protease (sspB)
Penicillin-binding protien 2 (mecA)
Exotoxin (SAUSA300_0407)
Triacylglycerol lipase (SAUSA300_0320)
Putative lipoprotein (SAUSA300_0079)
Bifunctional autolysin (atl)
Clumping factor B (clfB)
Uncharacterized protein (SAUSA300_pUSA010004)

Cell wall surface anchor family protein (SAUSA300_0136)
Putative lipoprotein (SAUSA300_0372)
Putative lipoprotein (SAUSA300_0769)
Immunodominant staphylococcal antigen B (isaB)
MAP domain-containing protein (SAUSA300_2164)
Probable transglycosylase IsaA (isaA)
Iron-regulated surface determinant protein C (isdC)
DUF4352 domain-containing protein (SAUSA300_1740)
Putative surface protein (SAUSA300_0883)
Non-specific serine/threonine protein kinase (pknB)
Iron-regulated surface determinant protein A (isdA)
Ear protein (ear)
Glutamine synthetase (glnA)
Lipoteichoic acid synthase (ltaS)
Immunoglobulin G-binding protein A (SAUSA300_0113)
Putative cell wall surface anchor family protein (SAUSA300_2436)
Probable CtpA-like serine protease (ctpA)
Staphylococcal enterotoxin K (sek)
Putative lipoprotein (SAUSA300_2355)
Elastin-binding protein EbpS (ebpS)
CHAP domain family protein (SAUSA300_0651)
Putative lipoprotein (SAUSA300_1478)
Fibrinogen-binding protein (efb)
Serine-aspartate repeat-containing protein D (sdrD)
Uncharacterized protein (SAUSA300_1759)
Putative lipoprotein (SAUSA300_0377)
Immunoglobulin-binding protein Sbi (sbi)
Staphylocoagulase (coa)
Glyceraldehyde-3-phosphate dehydrogenase (gap)
Foldase protein PrsA (prsA)
Iron compound ABC transporter, iron compound-binding protein SirA (sirA)
Oligopeptide ABC transporter, substrate-binding protein (oppA)
Serine-aspartate repeat-containing protein E (sdrE)
Glucose-6-phosphate isomerase (pgi)
Triosephosphate isomerase (tpiA)
5'-nucleotidase family protein (SAUSA300_0025)
Staphylococcal complement inhibitor (scn)

Transferrin receptor (SAUSA300_0721)
Catalase (katA)
Penicillin-binding protein 1 (pbpA)
Zinc metalloprotease (SAUSA300_1155)
Uncharacterized lipoprotein (SAUSA300_2315)
Glycine betaine aldehyde dehydrogenase (betA)
Fibronectin-binding protein A (fnbA)
Probable cell wall amidase LytH (lytH)
6,7-dimethyl-8-ribityllumazine synthase (ribH)
Putative surface protein (SAUSA300_0408)
tRNA uridine 5-carboxymethylaminomethyl modification enzyme MnmG (mnmG)
Fibronectin-binding protein B (fnbB)
Nucleoside disphosphate kinase (ndk)
Chemotaxis inhibitory protein (chp)
Truncated FmtB protein (fmtB)
Probable quinol oxidase subunit 2 (qoxA)
Iron-regulated surface determinant protein B (isdB)
Iron compound ABC transporter, iron compound-binding protein (SAUSA300_2235)
Uncharacterized peptidase (SAUSA300_1654)
Dihydrolipoyl dehydrogenase (lpdA)
Oligopeptide permease, peptide-binding protein (opp-1A)
Uncharacterized protein (SAUSA300_1031)
Uncharacterized protein (SAUSA300_2378)
General stress protein 20U (dps)
Putative phage infection protein (SAUSA300_2578)
Acetyl-coenzyme A carboxylase carboxyl transferase subunit beta (accD)
Uncharacterized protein (SAUSA300_2328)
Putative pyridoxal phosphate-dependent acyltransferase (SAUSA300_0535)
Serine protease HtrA-like protein (SAUSA300_0923)
ABC transporter, substrate-binding protein (SAUSA300_0618)
Uncharacterized protein (SAUSA300_0409)
Phi77 ORF006-like protein, putative capsid protein (SAUSA300_1938)
Cell shape-determining protein MreC (mreC)
Serine protease SplB (splB)
Exotoxin (SAUSA300_0395)
Serine protease HtrA-like protein (SAUSA300_1674)

Nuclease SbcCD subunit C (sbcC)
Ferric hydroxamate receptor (SAUSA300_1978)

Supplementary Table 2. Select examples of protein blast homology results for mature lipoprotein sequences of *SAUSA300_1739* and *SAUSA300_1740*.

MRSA gene	Blast protein result	Blast organism	%Identity	E-value
SAUSA300_1739	TNase-like domain-containing protein	*Paenisporosarcina* sp. HGH0030	47.9	2.80E-10
SAUSA300_1739	Nuclease	*Rossellomorea vietnamensis*	44.8	4.70E-10
SAUSA300_1739	DNA nuclease	*Peribacillus asahii*	48.5	5.50E-10
SAUSA300_1739	Thermonuclease	*Staphylococcus massiliensis* S46	56	4.60E-09
SAUSA300_1739	Thermonuclease	*Staphylococcus carnosus* (strain TM300)	38.8	7.60E-09
SAUSA300_1739	SPbeta prophage-derived endonuclease YokF	*Bacillus subtilis* (strain 168)	44.6	5.7E-08
SAUSA300_1740	Telomeric repeat-binding factor 2	*Staphylococcus saccharolyticus*	70.7	1.00E-33
SAUSA300_1740	Mpr protein	*Nonomuraea glycinis*	31	1.90E-12

Chapter Three: Summary of results and future directions

3.1 *Mycobacterium tuberculosis* uses ESX-1 and PDIM to prevent the development of protective Th17s

3.1.1 Summary of results

There is growing evidence that Mtb-infected humans with Th17s correlated with better control of Mtb infection compared to Mtb-infected humans without a Th17 response (16–18), non-human primates had gain control of Mtb in lung granulomas once Th17s arrived in the lungs (15), and several groups have shown that mice vaccinated to induce Th17s had better control of Mtb infection (20–22). Mtb has been shown to influence multiple host immune pathways all of which can impair Th17 differentiation. Mtb promotes lipoxin A4 production and suppresses the production of prostaglandin E2 to promote infection (90, 91), limits IL-12/23 p40 subunit expression (24), induces type I interferons (24, 28), and suppresses CD40 and DLL4 expression on antigen-presenting cells (92). In Chapter 2, we aimed to find out if Th17s and their signature cytokine IL-17a are protective during WT Mtb infection and why Th17s are not induced during WT Mtb infection in naïve unvaccinated mice.

The duration of WT Mtb infection or route of Mtb infection did not result in a change of the Th1-biased response in WT C57BL/6 (B6) mice. In *Tbet*$^{-/-}$ mice, Th17s were induced and these Th17s provided similar levels of protection compared to WT B6 mice with a Th1-biased response. The induced Th17s in *Tbet*$^{-/-}$ mice had protection mediated by IL-17a. Since Mtb ESX-1 and PDIM virulence factors have been shown to impact host production of immune cytokines that influence Th17 development, we hypothesized that Mtb uses the ESX-1 and PDIM virulence factors to suppress the differentiation of beneficial Th17s. Indeed, ESX-1 knockout and PDIM-lacking Mtb infections resulted in a loss of Th1s and gain in Th17s in the lungs of infected mice. Loss of another Mtb virulence factor, mmpL4, resulted in Mtb attenuation in the mouse lung; however, *mmpL4* knockout Mtb still induced Th1s and no Th17s indicating that the Th17 phenotype is a result of loss of ESX-1 or PDIM virulence factors, not attenuation of Mtb in general. Because ESX-1 and PDIM are known to be essential for inducing the detrimental type I interferon response in the host (24, 28), we then tested if mice lacking the ability to sense type I interferon (*Ifnar*$^{-/-}$) or had elevated levels of type I interferon (*Sp140*$^{-/-}$) (43) had changes in Th1s and Th17s induced during WT Mtb infection. Interestingly, *Ifnar*$^{-/-}$ mice lack the ability to sense type I interferons and had one-half the amount of Th1s induced compared to WT B6 mice, while *Sp140*$^{-/-}$ mice with elevated levels of type I interferons had twice the amount of Th1s induced compared to WT B6 mice. The loss of type I interferon signaling or elevation of type I interferons did not result in any change in the amount of Th17s. Lastly, we tested the professional antigen-presenting (dendritic) cells in the draining mediastinal lymph nodes of Mtb-infected mice. Similar to the Th1 and Th17 phenotypes seen in the lungs, WT and complemented Mtb strains induced higher amounts of IL-12 p35 in cDC1s and reduced amounts of IL-23 p19 in cDC2s compared

to ESX-1 knockout or PDIM-lacking Mtb infected mice. WT and complemented Mtb strains induced more Th1-polarizing cytokine IL-12 production in cDC1s and limited production of Th17-polarizing cytokine IL-23 in cDC2s compared to ESX-1 knockout or PDIM-lacking Mtb.

3.1.2 Future directions

The exact mechanism by which Mtb uses ESX-1 and PDIM to alter dendritic cell, and other professional phagocytes, expression of Th1-polarizing and Th17-polarizing cytokines and immune molecules remain unknown. ESX-1 and PDIM have been shown to permeabilize the host cell phagosome containing the intracellular bacteria (39), but the consequences of Mtb gaining access to the host cytosol are still not completely understood. Additionally, the role of each Mtb protein secreted through the ESX-1 secretion system is still not completely known. In the future, it would be important to identify all the changes in host cell cytosol and immune signaling impacted by ESX-1 and PDIM. One question not answered in this project is that ESX-1 knockout and PDIM-lacking Mtb infections are attenuated at first; however, a couple of months post-infection, the lung CFU of ESX-1 knockout or PDIM-lacking Mtb infected mice reach the same magnitude as WT Mtb infected mice. How is it that the weaker (ESX-1 knockout or PDIM-lacking) Mtb can eventually reach the same bacterial lung burden as WT Mtb? One hypothesis is that the immune system is dealing with a chronic infection at this later timepoint. Perhaps the newly made myeloid cells leaving the bone marrow are not completely differentiated and in a progenitor stage that is less antimicrobial. Another and non-exclusive answer could be that the T helper cells have become exhausted and are no longer producing enough antimicrobial and pro-inflammatory cytokines.

3.2 Identification of 2 novel nucleases secreted by Methicillin-resistant *Staphylococcus aureus* to promote virulency

3.2.1 Summary of results

Staphylococcus aureus is known to utilize a vast arsenal of secreted and surface-bound virulence factors. Although several *S. aureus* virulence factors have been identified and studied in-depth, there remain many *S. aureus* genes with unknown protein function and potential to be undiscovered virulence factors used by *S. aureus* to promote infection. We sought to find new virulence factors that *S. aureus* uses to contribute to infections and discover the protein functions of those new virulence factors.

We began with using mass spectrometry to find proteins that were more abundant in the culture filtrate than the cell pellet as the surface and secreted proteome from the North America-dominant methicillin-resistant *Staphylococcus aureus* (MRSA) strain USA300. The mass spectrometry experiment found 109 proteins that were more abundant in the culture filtrate than the cell pellet. Out of the 109 proteins, 29 proteins are uncharacterized and haven't been shown to contribute to *S. aureus* virulence in an in vivo

infection model. We tested 21 transposon mutants, out of the 29 uncharacterized protein hits available in a genome-wide non-essential-gene transposon arrayed library, using WT B6 bone-marrow-derived macrophage infection model to measure intracellular MRSA CFU and lactate dehydrogenase (LDH) release assay for macrophage cytotoxicity. We found 6 transposon-inserted mutants (*SAUSA300_1739, SAUSA300_1740, SAUSA300_0883, SAUSA300_2355, SAUSA300_0651,* and *SAUSA300_2315*) with modest differences in CFU and/or LDH compared to WT MRSA. Because *SAUSA300_1739* and *SAUSA300_1740* are located next to each other in the MRSA USA300 genome, we moved forward with these 2 hits. We found that *SAUSA300_1739* and *SAUSA300_1740* belong to an operon of 6 genes *SAUSA300_1739* to *SAUSA300_1744*. We show that knockouts of any of the 6 genes did not impact MRSA growth in pH 7.4, (acidic) pH 5.5, or (oxidative stress) 5 mM H_2O_2 LB broth. We then show that knockouts of any of the 6 genes resulted in MRSA attenuation in a murine subcutaneous infection model, while complementation rescued WT MRSA phenotype of higher bacterial burden and bigger lesion sizes. These results indicate that the *SAUSA300_1739* to *SAUSA300_1744* operon has 6 genes all of which are virulence factors. We then looked at the conservation of the *SAUSA300_1739* to *SAUSA300_1744* operon. We found that the *SAUSA300_1739* to *SAUSA300_1744* operon is highly conserved with >90% nucleotide identity amongst 55 *S. aureus* strains tested. Interestingly, the *SAUSA300_1741* and *SAUSA300_1742* genes split only in the MRSA USA300 lineage, while all other tested *S. aureus* strains have *SAUSA300_1741* and *SAUSA300_1742* as one open-reading frame. *SAUSA300_1739* and *SAUSA300_1740* have rough protein homology to nucleases, DNases, and DNA-binding proteins, so we purified SAUSA300_1739 and SAUSA300_1740 from BL21 *E. coli* cells and tested for DNase activity. We found that SAUSA300_1739 and SAUSA300_1740 both had DNase activity and degraded linear DNA, which was inhibited by the addition of EDTA.

3.2.2 Future directions

Staphylococcus aureus is known to secrete three nucleases to promote virulence. Nuc1 and EssD (also known as EsaD) are secreted, Nuc2 is surface-bound (65, 66). These nucleases have been shown to be essential for biofilm formation, degradation of antimicrobial neutrophil extracellular traps (NETs), and production of immunoinhibitory deoxyribonucleotides (65, 66, 89) allowing *S. aureus* to evade the immune system. We identified that *SAUSA300_1739* and *SAUSA300_1740* encode lipoproteins that have DNase activity. Future work should focus on how *SAUSA300_1739* and *SAUSA300_1740* promote MRSA infections, either by playing a role in NET degradation and/or biofilm formation or breakdown. A remaining question is do SAUSA300_1739 and SAUSA300_1740 have any unique mechanisms/functions that are not redundant to Nuc1, Nuc2, and/or EssD. If there is redundancy, then why does a single knockout in either SAUSA300_1739 or SAUSA300_1740 already attenuate MRSA in a murine

subcutaneous infection mode. Do these five nucleases have any unique roles and do they have different contributions depending on the type of MRSA infection?

The other four genes in the *SAUSA300_1739* to *SAUSA300_1744* operon remain to have unknown protein function. Future studies will need to discover the protein functions of *SAUSA300_1741* to *SAUSA300_1744* and find out how all 6 genes work together to promote MRSA virulency. In the MRSA USA300 strains used in this study, *SAUSA300_1741* and *SAUSA300_1742* have split into 2 genes. SAUSA300_1741 is another lipoprotein, while SAUSA300_1742 to SAUSA300_1744 are cytosolic proteins. What are the benefits of having *SAUSA300_1741* and *SAUSA300_1742* split into 2 separate proteins which majority of *S. aureus* strains have a *SAUSA300_1741-SAUSA300_1742* combined lipoprotein? Do *SAUSA300_1739*, *SAUSA300_1740*, and *SAUSA300_1741* form a complex together to degrade ribonucleotides? Additionally, what would happen if the signal peptides for *SAUSA300_1739* to *SAUSA300_1741* were altered to be secreted, but not lipoproteins? Why have membrane-bound lipoproteins that are nucleases?

References

1. World Health Organization, Global Tuberculosis Report 2022. *Geneva: World Health Organization. 2022. Global Tuberculosis Report 2022.* (2022). Available at: https://www.who.int/publications/i/item/9789240061729.
2. P. Kumar, Corrigendum: A perspective on the success and failure of BCG. *Front. Immunol.* **13**, 850325 (2022).
3. P. E. Fine, Variation in protection by BCG: implications of and for heterologous immunity. *Lancet* **346**, 1339–1345 (1995).
4. F. Zhou, D. Zhang, Recent advance in the development of tuberculosis vaccines in clinical trials and virus-like particle-based vaccine candidates. *Front. Immunol.* **14**, 1238649 (2023).
5. J. L. Flynn, *et al.*, An essential role for interferon gamma in resistance to Mycobacterium tuberculosis infection. *J. Exp. Med.* **178**, 2249–2254 (1993).
6. J.-L. Casanova, L. Abel, Genetic dissection of immunity to mycobacteria: the human model. *Annu. Rev. Immunol.* **20**, 581–620 (2002).
7. M. D. Tameris, *et al.*, Safety and efficacy of MVA85A, a new tuberculosis vaccine, in infants previously vaccinated with BCG: a randomised, placebo-controlled phase 2b trial. *Lancet* **381**, 1021–1028 (2013).
8. B. Zhang, *et al.*, Association between IL-18, IFN-γ and TB susceptibility: a systematic review and meta-analysis. *Ann. Palliat. Med.* **10**, 10878–10886 (2021).
9. L. Guglani, S. A. Khader, Th17 cytokines in mucosal immunity and inflammation. *Curr. Opin. HIV AIDS* **5**, 120–127 (2010).
10. S. L. Gaffen, Structure and signalling in the IL-17 receptor family. *Nat. Rev. Immunol.* **9**, 556–567 (2009).
11. V. Lazarevic, *et al.*, T-bet represses T(H)17 differentiation by preventing Runx1-mediated activation of the gene encoding RORγt. *Nat. Immunol.* **12**, 96–104 (2011).
12. M. Pepper, *et al.*, Different routes of bacterial infection induce long-lived TH1 memory cells and short-lived TH17 cells. *Nat. Immunol.* **11**, 83–89 (2010).
13. W.-I. Yeh, I. L. McWilliams, L. E. Harrington, IFNγ inhibits Th17 differentiation and function via Tbet-dependent and Tbet-independent mechanisms. *J. Neuroimmunol.* **267**, 20–27 (2014).
14. B. Guo, E. Y. Chang, G. Cheng, The type I IFN induction pathway constrains Th17-mediated autoimmune inflammation in mice. *J. Clin. Invest.* **118**, 1680–1690 (2008).
15. H. P. Gideon, *et al.*, Multimodal profiling of lung granulomas in macaques reveals cellular correlates of tuberculosis control. *Immunity* **55**, 827-846.e10 (2022).
16. P. Ogongo, *et al.*, High-parameter phenotypic characterization reveals a subset of human Th17 cells that preferentially produce IL-17 against M. tuberculosis antigen. *Front. Immunol.* **15**, 1378040 (2024).
17. M. Sun, *et al.*, Specific CD4+ T cell phenotypes associate with bacterial control in people who “resist” infection with Mycobacterium tuberculosis. *Nat. Immunol.* **25**, 1411–1421 (2024).
18. A. Nathan, *et al.*, Multimodally profiling memory T cells from a tuberculosis cohort identifies cell state associations with demographics, environment and disease. *Nat. Immunol.* **22**, 781–793 (2021).

19. R. Gopal, *et al.*, Unexpected role for IL-17 in protective immunity against hypervirulent Mycobacterium tuberculosis HN878 infection. *PLoS Pathog.* **10**, e1004099 (2014).
20. S. A. Khader, *et al.*, IL-23 and IL-17 in the establishment of protective pulmonary CD4+ T cell responses after vaccination and during Mycobacterium tuberculosis challenge. *Nat. Immunol.* **8**, 369–377 (2007).
21. N. Aguilo, *et al.*, Pulmonary but not subcutaneous delivery of BCG vaccine confers protection to tuberculosis-susceptible mice by an interleukin 17-dependent mechanism. *J. Infect. Dis.* **213**, 831–839 (2016).
22. R. M. Jong, *et al.*, Mucosal vaccination with cyclic dinucleotide adjuvants induces effective T cell homing and IL-17-dependent protection against Mycobacterium tuberculosis infection. *J. Immunol.* **208**, 407–419 (2022).
23. S. A. Stanley, S. Raghavan, W. W. Hwang, J. S. Cox, Acute infection and macrophage subversion by Mycobacterium tuberculosis require a specialized secretion system. *Proc. Natl. Acad. Sci. U. S. A.* **100**, 13001–13006 (2003).
24. S. A. Stanley, J. E. Johndrow, P. Manzanillo, J. S. Cox, The Type I IFN response to infection with Mycobacterium tuberculosis requires ESX-1-mediated secretion and contributes to pathogenesis. *J. Immunol.* **178**, 3143–3152 (2007).
25. R. O. Watson, *et al.*, The cytosolic sensor cGAS detects Mycobacterium tuberculosis DNA to induce type I interferons and activate autophagy. *Cell Host Microbe* **17**, 811–819 (2015).
26. R. O. Watson, P. S. Manzanillo, J. S. Cox, Extracellular M. tuberculosis DNA targets bacteria for autophagy by activating the host DNA-sensing pathway. *Cell* **150**, 803–815 (2012).
27. J. S. Cox, B. Chen, M. McNeil, W. R. Jacobs Jr, Complex lipid determines tissue-specific replication of Mycobacterium tuberculosis in mice. *Nature* **402**, 79–83 (1999).
28. A. K. Barczak, *et al.*, Systematic, multiparametric analysis of Mycobacterium tuberculosis intracellular infection offers insight into coordinated virulence. *PLoS Pathog.* **13**, e1006363 (2017).
29. A. Schlitzer, *et al.*, IRF4 transcription factor-dependent CD11b+ dendritic cells in human and mouse control mucosal IL-17 cytokine responses. *Immunity* **38**, 970–983 (2013).
30. P. Soldevilla, C. Vilaplana, P.-J. Cardona, Mouse models for Mycobacterium tuberculosis pathogenesis: Show and do not tell. *Pathogens* **12**, 49 (2022).
31. P. Andersen, A. B. Andersen, A. L. Sørensen, S. Nagai, Recall of long-lived immunity to Mycobacterium tuberculosis infection in mice. *J. Immunol.* **154**, 3359–3372 (1995).
32. A. Bekmurzayeva, M. Sypabekova, D. Kanayeva, Tuberculosis diagnosis using immunodominant, secreted antigens of Mycobacterium tuberculosis. *Tuberculosis (Edinb.)* **93**, 381–388 (2013).
33. M. Karbalaei Zadeh Babaki, S. Soleimanpour, S. A. Rezaee, Antigen 85 complex as a powerful Mycobacterium tuberculosis immunogene: Biology, immune-pathogenicity, applications in diagnosis, and vaccine design. *Microb. Pathog.* **112**, 20–29 (2017).
34. T. Dileepan, *et al.*, Robust antigen specific th17 T cell response to group A Streptococcus is dependent on IL-6 and intranasal route of infection. *PLoS Pathog.* **7**, e1002252 (2011).

35. D. Sleep, J. Cameron, L. R. Evans, Albumin as a versatile platform for drug half-life extension. *Biochim. Biophys. Acta* **1830**, 5526–5534 (2013).
36. B. M. Sullivan, *et al.*, Increased susceptibility of mice lacking T-bet to infection with Mycobacterium tuberculosis correlates with increased IL-10 and decreased IFN-gamma production. *Mian Yi Xue Za Zhi* **175**, 4593–4602 (2005).
37. M. A. Sallin, *et al.*, Th1 Differentiation Drives the Accumulation of Intravascular, Non-protective CD4 T Cells during Tuberculosis. *Cell Rep.* **18**, 3091–3104 (2017).
38. A. E. Hinman, *et al.*, Mycobacterium tuberculosis canonical virulence factors interfere with a late component of the TLR2 response. *Elife* **10** (2021).
39. J. Augenstreich, *et al.*, ESX-1 and phthiocerol dimycocerosates of Mycobacterium tuberculosis act in concert to cause phagosomal rupture and host cell apoptosis. *Cell. Microbiol.* **19** (2017).
40. T. D. Crosskey, K. S. H. Beckham, M. Wilmanns, The ATPases of the mycobacterial type VII secretion system: Structural and mechanistic insights into secretion. *Prog. Biophys. Mol. Biol.* **152**, 25–34 (2020).
41. R. M. Wells, *et al.*, Discovery of a siderophore export system essential for virulence of Mycobacterium tuberculosis. *PLoS Pathog.* **9**, e1003120 (2013).
42. V. S. Ramgolam, Y. Sha, J. Jin, X. Zhang, S. Markovic-Plese, IFN-beta inhibits human Th17 cell differentiation. *J. Immunol.* **183**, 5418–5427 (2009).
43. D. X. Ji, *et al.*, Role of the transcriptional regulator SP140 in resistance to bacterial infections via repression of type I interferons. *Elife* **10** (2021).
44. C. Dye, P. Glaziou, K. Floyd, M. Raviglione, Prospects for tuberculosis elimination. *Annu. Rev. Public Health* **34**, 271–286 (2013).
45. S. Sakai, *et al.*, CD4 T cell-derived IFN-γ plays a minimal role in control of pulmonary Mycobacterium tuberculosis infection and must be actively repressed by PD-1 to prevent lethal disease. *PLoS Pathog.* **12**, e1005667 (2016).
46. I. Comas, *et al.*, Human T cell epitopes of Mycobacterium tuberculosis are evolutionarily hyperconserved. *Nat. Genet.* **42**, 498–503 (2010).
47. P. Ogongo, *et al.*, Rare Variable M. tuberculosis Antigens induce predominant Th17 responses in human infection. *bioRxivorg* (2024).
48. F. McNab, K. Mayer-Barber, A. Sher, A. Wack, A. O'Garra, Type I interferons in infectious disease. *Nat. Rev. Immunol.* **15**, 87–103 (2015).
49. S. L. Gaffen, R. Jain, A. V. Garg, D. J. Cua, The IL-23-IL-17 immune axis: from mechanisms to therapeutic testing. *Nat. Rev. Immunol.* **14**, 585–600 (2014).
50. G. L. Stritesky, N. Yeh, M. H. Kaplan, IL-23 promotes maintenance but not commitment to the Th17 lineage. *J. Immunol.* **181**, 5948–5955 (2008).
51. J. G. Krueger, *et al.*, IL-23 past, present, and future: a roadmap to advancing IL-23 science and therapy. *Front. Immunol.* **15**, 1331217 (2024).
52. L. Solans, *et al.*, A specific polymorphism in Mycobacterium tuberculosis H37Rv causes differential ESAT-6 expression and identifies WhiB6 as a novel ESX-1 component. *Infect. Immun.* **82**, 3446–3456 (2014).
53. R. Stadhouders, E. Lubberts, R. W. Hendriks, A cellular and molecular view of T helper 17 cell plasticity in autoimmunity. *J. Autoimmun.* **87**, 1–15 (2018).
54. G. G. Mahairas, P. J. Sabo, M. J. Hickey, D. C. Singh, C. K. Stover, Molecular analysis of genetic differences between Mycobacterium bovis BCG and virulent M. bovis. *J. Bacteriol.* **178**, 1274–1282 (1996).

55. T. Hsu, *et al.*, The primary mechanism of attenuation of bacillus Calmette–Guérin is a loss of secreted lytic function required for invasion of lung interstitial tissue. *Proc. Natl. Acad. Sci. U. S. A.* **100**, 12420–12425 (2003).
56. A. Arbues, *et al.*, Construction, characterization and preclinical evaluation of MTBVAC, the first live-attenuated M. tuberculosis-based vaccine to enter clinical trials. *Vaccine* **31**, 4867–4873 (2013).
57. K. Dijkman, *et al.*, Pulmonary MTBVAC vaccination induces immune signatures previously correlated with prevention of tuberculosis infection. *Cell Rep. Med.* **2**, 100187 (2021).
58. W. C. Noble, H. A. Valkenburg, C. H. Wolters, Carriage of Staphylococcus aureus in random samples of a normal population. *J. Hyg. (Lond.)* **65**, 567–573 (1967).
59. M. W. Casewell, R. L. R. Hill, The carrier state: methicillin-resistant Staphylococcus aureus. *J. Antimicrob. Chemother.* **18**, 1–12 (1986).
60. W. R. Miller, C. A. Arias, ESKAPE pathogens: antimicrobial resistance, epidemiology, clinical impact and therapeutics. *Nat. Rev. Microbiol.* **22**, 598–616 (2024).
61. CDC, 2019 Antibiotic Resistance Threats Report. *Antimicrobial Resistance* (2025). Available at: https://www.cdc.gov/antimicrobial-resistance/data-research/threats/index.html [Accessed 28 November 2025].
62. S. Y. C. Tong, J. S. Davis, E. Eichenberger, T. L. Holland, V. G. Fowler Jr, Staphylococcus aureus infections: epidemiology, pathophysiology, clinical manifestations, and management. *Clin. Microbiol. Rev.* **28**, 603–661 (2015).
63. D. J. Diekema, *et al.*, Continued emergence of USA300 methicillin-resistant Staphylococcus aureus in the United States: results from a nationwide surveillance study. *Infect. Control Hosp. Epidemiol.* **35**, 285–292 (2014).
64. G. Y. C. Cheung, J. S. Bae, M. Otto, Pathogenicity and virulence of Staphylococcus aureus. *Virulence* **12**, 547–569 (2021).
65. J. Yu, *et al.*, Thermonucleases contribute to Staphylococcus aureus biofilm formation in implant-associated infections-A redundant and complementary story. *Front. Microbiol.* **12**, 687888 (2021).
66. R. J. Ohr, M. Anderson, M. Shi, O. Schneewind, D. Missiakas, EssD, a nuclease effector of the Staphylococcus aureus ESS pathway. *J. Bacteriol.* **199**, e00528-16 (2017).
67. J. Cox, M. Mann, MaxQuant enables high peptide identification rates, individualized p.p.b.-range mass accuracies and proteome-wide protein quantification. *Nat. Biotechnol.* **26**, 1367–1372 (2008).
68. G. Teo, *et al.*, SAINTexpress: improvements and additional features in Significance Analysis of INTeractome software. *J. Proteomics* **100**, 37–43 (2014).
69. R. Tian, B. Imanian, VBCG: 20 validated bacterial core genes for phylogenomic analysis with high fidelity and resolution. *Microbiome* **11**, 247 (2023).
70. I. R. Monk, J. J. Tree, B. P. Howden, T. P. Stinear, T. J. Foster, Complete bypass of restriction systems for major staphylococcus aureus lineages. *MBio* **6**, e00308-15 (2015).
71. N. W. M. de Jong, T. van der Horst, J. A. G. van Strijp, R. Nijland, Fluorescent reporters for markerless genomic integration in Staphylococcus aureus. *Sci. Rep.* **7** (2017).

72. Y. Perez-Riverol, *et al.*, The PRIDE database at 20 years: 2025 update. *Nucleic Acids Res.* **53**, D543–D553 (2025).
73. Z. R. Tranchemontagne, R. B. Camire, V. J. O'Donnell, J. Baugh, K. M. Burkholder, Staphylococcus aureus strain USA300 perturbs acquisition of lysosomal enzymes and requires phagosomal acidification for survival inside macrophages. *Infect. Immun.* **84**, 241–253 (2015).
74. P. D. Fey, *et al.*, A genetic resource for rapid and comprehensive phenotype screening of nonessential Staphylococcus aureus genes. *MBio* **4**, e00537-12 (2013).
75. F. Jacob, J. Monod, Genetic regulatory mechanisms in the synthesis of proteins. *J. Mol. Biol.* **3**, 318–356 (1961).
76. A. de Jong, H. Pietersma, M. Cordes, O. P. Kuipers, J. Kok, PePPER: a webserver for prediction of prokaryote promoter elements and regulons. *BMC Genomics* **13**, 299 (2012).
77. A. Gupta, RT-PCR: characterization of long multi-gene operons and multiple transcript gene clusters in bacteria. *Biotechniques* **27**, 966–70, 972 (1999).
78. I. R. Monk, I. M. Shah, M. Xu, M.-W. Tan, T. J. Foster, Transforming the untransformable: application of direct transformation to manipulate genetically Staphylococcus aureus and Staphylococcus epidermidis. *MBio* **3** (2012).
79. J. A. Lindsay, M. T. G. Holden, Staphylococcus aureus: superbug, super genome? *Trends Microbiol.* **12**, 378–385 (2004).
80. R. Dehbanipour, Z. Ghalavand, Anti-virulence therapeutic strategies against bacterial infections: recent advances. *Germs* **12**, 262–275 (2022).
81. J. L. Telford, Bacterial genome variability and its impact on vaccine design. *Cell Host Microbe* **3**, 408–416 (2008).
82. J.-A. McClure, K. Zhang, Complete genome sequences of two USA300-related community-associated methicillin-resistant Staphylococcus aureus clinical isolates. *Microbiol. Resour. Announc.* **8**, e00404-19 (2019).
83. J. S. Wiberg, On the mechanism of metal activation of deoxyribobuclease I. *Arch. Biochem. Biophys.* **73**, 337–358 (1958).
84. L. M. Hellman, M. G. Fried, Electrophoretic mobility shift assay (EMSA) for detecting protein-nucleic acid interactions. *Nat. Protoc.* **2**, 1849–1861 (2007).
85. J. Kluytmans, A. van Belkum, H. Verbrugh, Nasal carriage of Staphylococcus aureus: epidemiology, underlying mechanisms, and associated risks. *Clin. Microbiol. Rev.* **10**, 505–520 (1997).
86. S. Kitamoto, H. Nagao-Kitamoto, P. Kuffa, N. Kamada, Regulation of virulence: the rise and fall of gastrointestinal pathogens. *J. Gastroenterol.* **51**, 195–205 (2016).
87. X. Xiao, Y. Li, L. Li, Y. Q. Xiong, Identification of methicillin-resistant Staphylococcus aureus (MRSA) genetic factors involved in human endothelial cells damage, an important phenotype correlated with persistent endovascular infection. *Antibiotics (Basel)* **11**, 316 (2022).
88. M. R. Grosser, *et al.*, Genetic requirements for Staphylococcus aureus nitric oxide resistance and virulence. *PLoS Pathog.* **14**, e1006907 (2018).
89. V. Thammavongsa, D. M. Missiakas, O. Schneewind, Staphylococcus aureus degrades neutrophil extracellular traps to promote immune cell death. *Science* **342**, 863–866 (2013).

90. V. Kaul, *et al.*, An important role of prostanoid receptor EP2 in host resistance to Mycobacterium tuberculosis infection in mice. *J. Infect. Dis.* **206**, 1816–1825 (2012).
91. S. M. Behar, M. Divangahi, H. G. Remold, Evasion of innate immunity by Mycobacterium tuberculosis: is death an exit strategy? *Nat. Rev. Microbiol.* **8**, 668–674 (2010).
92. A. B. Enriquez, *et al.*, Mycobacterium tuberculosis impedes CD40-dependent notch signaling to restrict Th17 polarization during infection. *iScience* **25**, 104305 (2022).